

EE0007345.000

M3 Wave LLC

Improved Survivability and Lower Cost in Submerged Wave Energy Device

PI: Mike Morrow

Team Members:

Dr. Michael Delos-Reyes	M3 Wave
Alice Gillespie	M3 Wave
Ryan G. Coe	Sandia National Labs
Chris Chartrand	Sandia National Labs
Fabian Wendt	National Renewable Energy Lab
Tuba Ozkan-Haller	Oregon State University
Pedro Lomonaco	Oregon State University
Yi-Hsiang Yu	National Renewable Energy Lab
Jesse Roberts	Sandia National Labs
Sterling Olson	Sandia National Labs
Craig Jones	Integral Consulting, Inc.
Steve Spencer	Ershigs

Executive Summary:

This project successfully developed methods for numerical modeling of sediment transport phenomena around rigid objects resting on or near the ocean floor. These techniques were validated with physical testing using actual sediment in a large wave tank. These methods can be applied to any nearshore structure, including wave energy devices including surge devices and hinged flap systems. These techniques can be used to economically iterate on device geometries, lowering the cost to refine designs and reducing time to market.

The key takeaway for this project was that the most cost-effective method to reduce sediment transport impact is to avoid it altogether. By elevating device structures slightly off the seabed, sediment particles will flow under and around, ebbing and flowing naturally. This allows sediment scour and accretion to follow natural equalization processes without hydrodynamic acceleration or deceleration effects of artificial structures.

Acknowledgment: "This material is based upon work supported by the Department of Energy's Office of Energy Efficiency and Renewable Energy (EERE) under the [enter Program or initiative name] under Award Number(s) [enter the award number(s)]."

Disclaimer: "This report was prepared as an account of work sponsored by an agency of the United States Government. Neither the United States Government nor any agency thereof, nor any of their employees, makes any warranty, express or implied, or assumes any legal liability or responsibility for the accuracy, completeness, or usefulness of any information, apparatus, product, or process disclosed, or represents that its use would not infringe privately owned rights. Reference herein to any specific commercial product, process, or service by trade name, trademark, manufacturer, or otherwise does not necessarily constitute or imply its endorsement, recommendation, or favoring by the United States Government or any agency thereof. The views and opinions of authors expressed herein do not necessarily state or reflect those of the United States Government or any agency thereof."

Contents

I. Final Report Introduction / Purpose.....	4
Introduction	4
Purpose	4
General Plan	4
II. Numerical Modeling SubReport (SNL and NREL).	5
Introduction	5
Generalized modes analysis	6
Defining an empirical scour trend.....	7
Results	9
Conclusion.....	13
III. Numerical Modeling SubReport (M3)	14
Objective	14
Numerical Model.....	14
Utilizing CFD Simulations to Predict Scour	16
Theoretical Basis of CFD-Based Scour Predictions	16
Scour Model Validation.....	17
Model Validation Runs.....	20
Effects of Geometry	27
Analysis.....	31
Conclusions	32
IV. Experimental Lab Work (Empirical Testing)- Laboratory Experiments at 1:25 Scale.....	33
Introduction	33
Experimental Methods	33
Results	34
Analysis / Conclusions	35
V. Experimental Lab Work (Empirical Testing)- Laboratory Experiments at 1:5 Scale	36
Introduction	36
Experimental Methods	36
Results	44
Influence of Wave Conditions.....	44
Influence of Caisson geometry.....	45
Influence of elevation off bottom.....	46
Influence of Device Orientation.....	47
Influence of Test Apparatus.....	47

Next-Generation Design.....	48
Analysis / Conclusions	48
References	50
Publications associated with this project:.....	51
Appendix A	53
Appendix B: FEA of Composite version of APEX.....	63

I. Final Report Introduction / Purpose

Introduction

Submerged pressure differential (SPD) type wave energy converters (WECs) have been shown to successfully extract useful amounts of electricity from ocean waves [1,2,3]. The Delos-Reyes Morrow Pressure Device (DMP), currently being commercialized by M3 Wave LLC under the name “APEX,” is an example of one such SPD. Extensive testing at 1:50th and 1:6th scale in wave tanks led to a 2014 open water test in the Pacific Ocean off the coast of Oregon. This testing uncovered a challenge to the survivability of the system: sediment transport. Sediment transport presents a serious survivability risk for APEX due to the risk of scour and accretion causing device pitch or roll, resulting in loss of efficiency and eventual shut down. Additionally, as an alternative to mooring, APEX used ballast weight to remain stationary on the ocean floor. This will result in significant capital and deployment cost increases in larger deployments. During this project, M3 Wave explored integration of various structural geometries to mitigate sediment transport as well as utilization of alternate materials (composites) as a cost-effective way to enable these geometries.

Purpose

The objective of this project was to develop a set of analysis tools (hydrodynamics and structural models providing inputs into a sediment model), and use those tools to identify and refine the optimal device geometry for APEX that will improve robustness and survivability while improving LCOE (levelized cost of energy) by reducing CAPEX (capital expenditure) and increasing AEP (Annual Energy Production).

General Plan

The project was divided into numerical modeling and scale testing phases. The numerical modeling team members identified two different approaches to predicting sediment transport around a submerged near-shore structure. To explore both of these approaches and to provide cross-validation, the modeling team further divided into a National Labs group and an M3 group. Each team, using slightly different scientific/numerical approaches, performed numerical modeling of sediment transport near a default APEX device and evaluated correlation to empirical results. Those reports are included here in their respective sections and include testing results and correlation observations. More detail around physical testing methods and results is included in the subsequent scale testing section.

During the downselect phase, the modeling teams provided insights into avenues that did not warrant further exploration. At times this was supported by cursory numerical modeling runs to provide trends or extrapolations of the potential success- or failure- of the various design concepts.

II. Numerical Modeling SubReport (SNL and NREL).

Introduction

This portion of the report focuses on the investigation of scour beneath the M3 WAVE APEX wave energy converter (WEC). The pressure differential concept for a WEC, as implemented in the M3 design, is based on two flexible air-bags that are connected through a tube [1]. The bags inflate and deflate, depending on the local wave induced forces on the bags. This triggers a flow through the connecting tube. A turbine in the middle of the tube is driven by this airflow and produces electrical power.

In an initial at-sea deployment of a demonstration/experimental APEX in September 2014 off the coast of Oregon, scour beneath the device was observed. As sediment from the beneath the device was removed by scour, the device's pitch orientation was shifted. This change in pitch orientation caused a degradation in power performance.

To assess scour for the APEX device (as well as future similar devices), numerical and experimental efforts were undertaken. First, two different causes of scour for the APEX were considered: (1) wave induced/diffracted flow and (2) radiated flow due to the motion of the APEX device. Next, using the canonical scour system of oscillatory two-dimensional flow over a pipe, a relationship based on local shear stress on the sea bed was developed. Experiments with a series of APEX-like devices were carried out to assess scour. Predictions from this formulation were compared with experimental results and show good agreement on local scour depth and overall scour area.

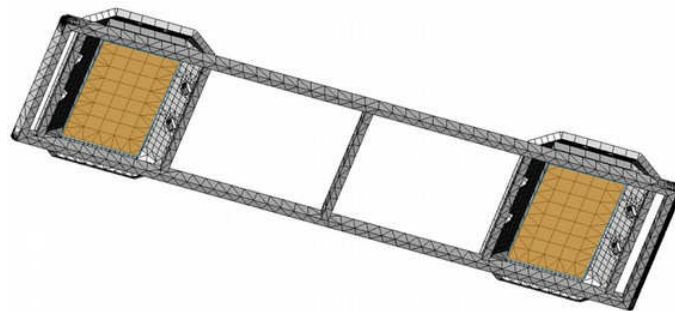


Figure 1: M3 WAVE APEX device geometry used for WAMIT Model.

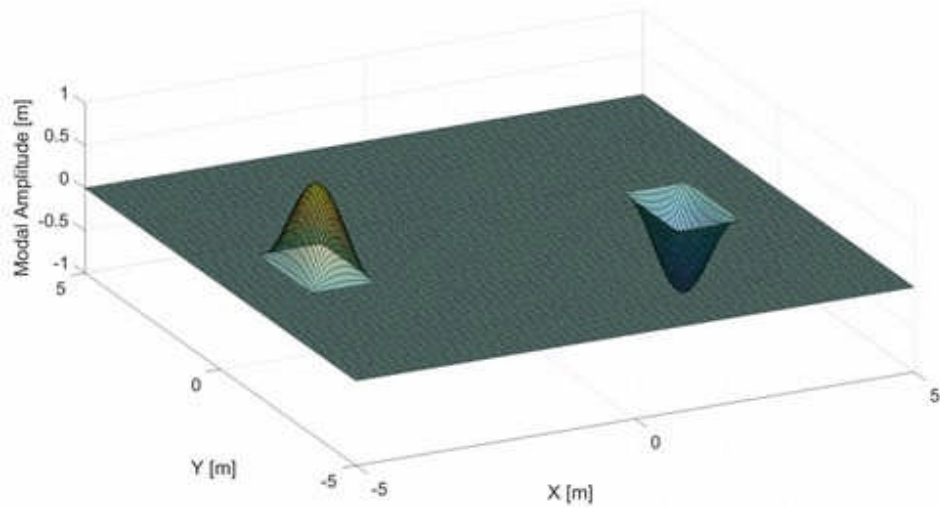


Figure 2: Mode Shape introduced to consider bag motion in WAMIT model.

Generalized modes analysis

To assess the importance of radiated versus incident/diffracted flow for scour, the M3 Apex device was modeled within WAMIT [4]. This approach can be used to assess the relative importance of radiated versus incident/diffracted flow, but does not include viscous effects. Thus WAMIT was not used in this study to directly predict scour.

The flexible bag motion of the APEX was considered through the introduction of one additional generalized mode. The utilized surface mesh is shown in Figure 1. The additional mode shape used to represent the bag motion is shown in Figure 2. This mode shape is applied to the bottom surfaces of the flexible bags, highlighted in orange in Figure 1. No additional stiffness/mass/damping were associated with the introduced bag deformation mode.

Regime	$T_{p,1}$ [s]	$T_{p,2}$ [s]	$H_{s,1}$ [m]	$H_{s,2}$ [m]
1	16.3	6.92	0.38	0.49
2	8.33	14.44	0.90	0.37
3	11.11	4.47	0.30	0.31
4	13.07	20.00	1.04	0.50

Table 1: Wave regimes used in WAMIT analyses.

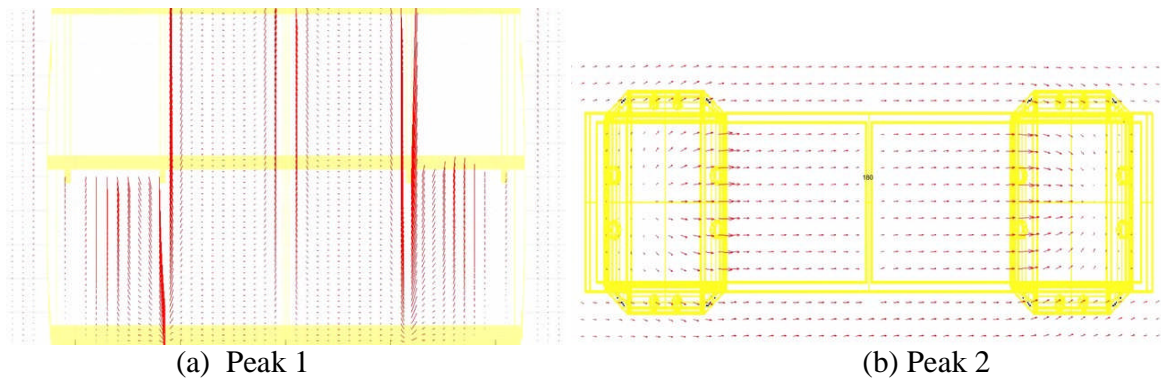


Figure 3: Flow field around APEX device predicted by WAMIT for Regime 3.

Four bimodal wave regimes that occurred during the Apex Oregon deployment were selected for analysis with WAMIT (Table 1). The APEX device was simulated in WAMIT using these four selected wave regimes. The flow field around the body was requested as output and further analyzed in terms of scouring potential. The resulting flow field around the device is visualized at the seabed level in Figure 3a and at a length-wise cross section along the center in Figure 3b for Regime 3.

The maximum velocities occur at the gap between seabed and caisson (orange circles in Figure 3). The simulation was repeated with a rigid bag and the flow fields with and without flexible bags were compared (Figure 4). In conclusion, the influence of the bag motion on flow field close to seabed appears to be relatively small and is therefore not considered a driving factor for any potential scouring.

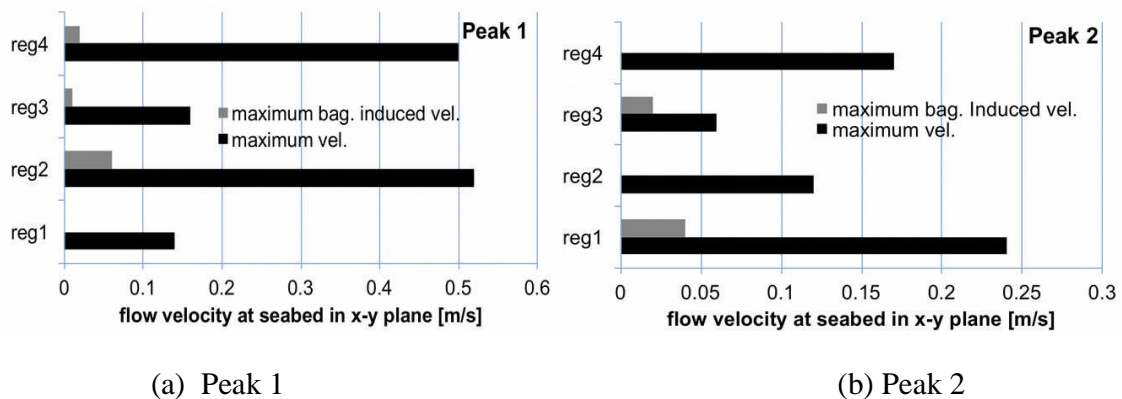


Figure 4. Maximum flow velocities at seabed.

Defining an empirical scour trend

A number of studies have used computational fluid dynamics (CFD) to predict scour. Generally, the methods developed use some sort of iterative/coupled approach to allow for scour to develop (see,

e.g., [2, 5]). Geometries in the CFD simulations are thus deformed to represent the scour process. This allows the flow field to respond, just as in a real scour process.

In this study, we have pursued a method which might approximate/predict scour with fewer computational resources. For this purpose, we utilized shear stress on the sea floor (e.g., from a CFD simulation). To predict scour underneath an arbitrary geometry, we have examined the flow over a 2-dimensional (2D) pipe. The relationship derived via this canonical case can then be extended to arbitrary geometries. The 2D pipe flow problem is well-studied and empirical data has shown a strong trend [3].

$$\frac{S}{D} = 0.1 \sqrt{KC}$$

(1)

The Keulegan-Carpenter number, KC, is given by

$$KC = \frac{UT}{D}$$

(2)

Similarly to the trend given by (1), the scour width for 2D pipe flow follows.

(In the development of this work, a set of simulations were conducted to investigate 2D pipe scour. A summary of these results is presented in Appendix XXX.)

$$\frac{W}{D} = 0.35 KC^{0.65}$$

(3)

Knowing that scour is highly dependent on KC, it is desirable to define an empirical trend that will allow local scour to be predicted by some function of KC. We thus define local Keulegan-Carpenter number as

$$KC(x, y) = \frac{T}{D} \left(\frac{\tau(x, y) - \tau_\infty}{\rho U_m} \right)$$

(4)

Here, T is the wave period. The parameter D is some representative dimension of the body of interest. The local shear stress is given by $\tau(x, y)$ and τ_∞ is the far field shear stress. The water density is given by ρ and the far field flow velocity is U_m .

In addition to KC, scour in waves is known to be influenced by turbulence levels. By monitoring the turbulence level just above the floor, we can write

$$D_{TKE}(x, y) = \frac{D \sqrt[3]{TKE(x, y)}}{U_m}$$

(5)

Here, $TKE(x, y)$ is the turbulent kinetic energy level averaged over one period taken at 1 cm above the floor. The tuning parameter f_{cal} will be defined momentarily.

Using (4) and (5), the local scour can be predicted by

$$S(x, y) = D_{TKE} \sqrt[3]{C(x, y)} - S_{\infty} \quad (6)$$

where S_{∞} is the far field scour. The tuning parameter f_{cal} in (5) can be set based on the known solution for 2D pipe flow.

$$f_{cal}(H_s, T_p) = \operatorname{argmin}(|\max(S(x, y)) - S_{pipe}|) \quad (7)$$

Here, S_{pipe} is the scour depth prediction from (1).

Wave ID	Height, H [m]	Period, T [s]	Wave length, λ [m]
1	0.30	3.6	15.9
2	0.30	5.8	28.2
3	0.60	3.6	15.9
4	0.60	5.8	28.2

Table 2: Wave conditions for comparison between CFD scour prediction and experimental data.

Results

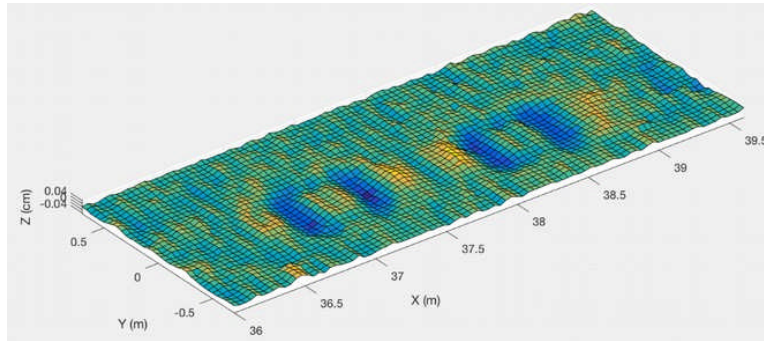
A series of experiments were run in the Oregon State University (OSU) Large Wave Flume using scale models of APEX and sand. The flume is 104 m long and 3.7 m wide. For these tests, a water depth of 2.7 m was used. Waves in the flume are produced by a piston-type wave maker. Table 2 lists the wave conditions considered here.

For each wave, sonar was used to measure the local scour before and after running waves. The difference between the measurements was taken to find the scour created during the experiment. The resulting surfaces are shown in Figure 5. CFD simulations were run to correspond with each wave.

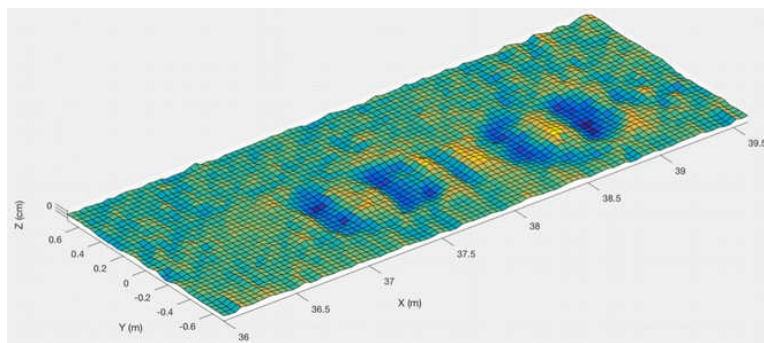
To provide a comparison between the experimental and CFD-based scour results, a longitudinal transect was taken down the center of the APEX device. Thus, the local scour ($S(x, y = 0)$) can be plotted from both the experiment and CFD prediction. The resulting comparison is shown for each wave from Table 2 in Figure 6.

Overall, the comparisons shown in Figure 6 display good agreement between the CFD scour prediction and the experimental results. The predictions in Wave 1 and Wave 2 are best. Here, the local scour depth prediction matches the experiment quite well. The prediction perform worse in Waves 3 and 4, which have double the amplitude of Waves 1 and 2. However, even when the CFD scour prediction is poor (in Waves 3 and 4), while the local scour *depth* may not be well-predicted, the *extents of the scour* tend to match fairly well.

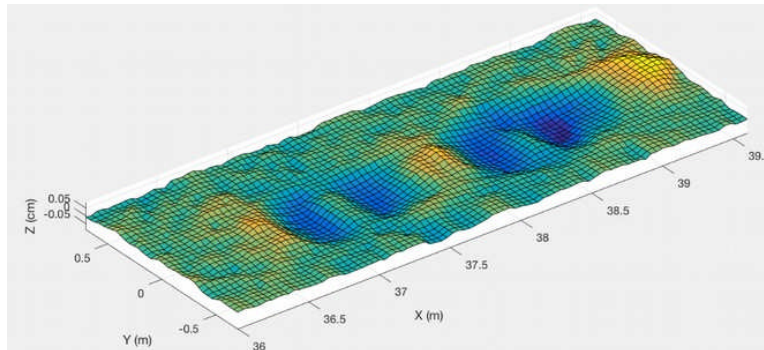
One factor that may have affected the results is the presence of some non-zero initial scour. In the case of Wave 4 the initial scour was quite large, which may have compromised the experiment. Also, the device may not always have been located exactly the same in the experimental and numerical tests.



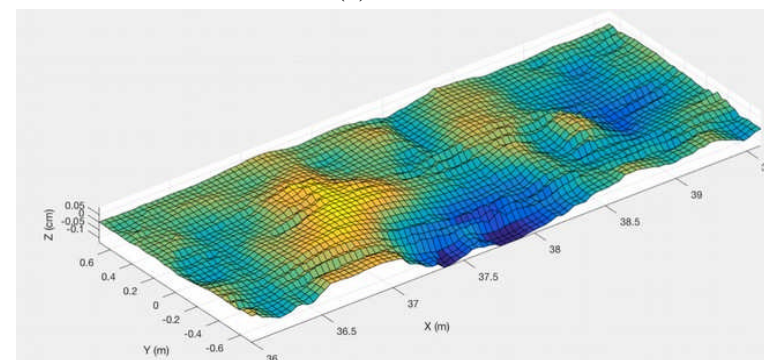
(a) Wave 1



(b) Wave 2



(c) Wave 3



(d) Wave 4

Figure 5: Experimental measured scour for APEX device.

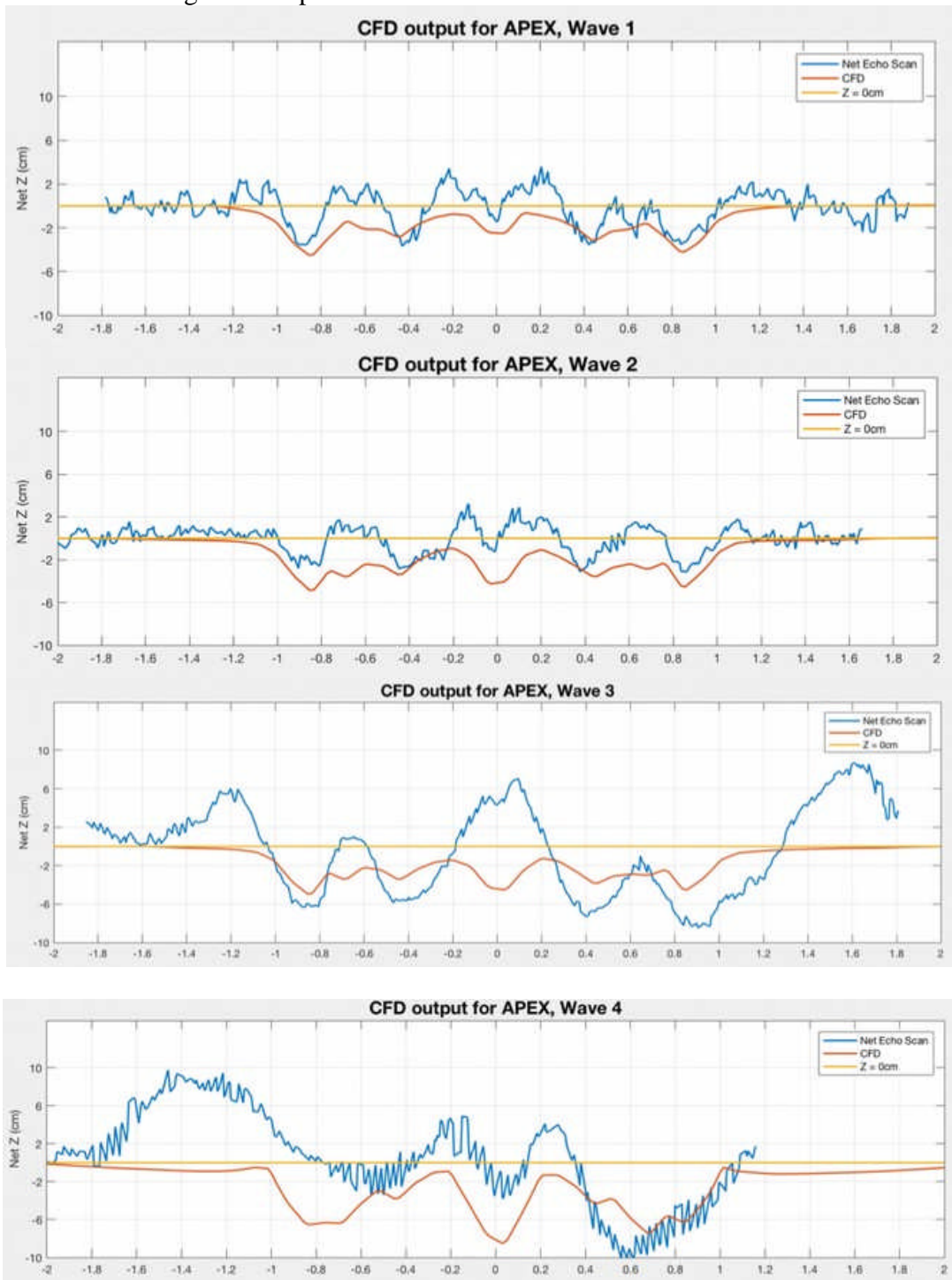


Figure 6: Comparison of scour from experiment and CFD prediction using (6) for APEX device. Plot of longitudinal transect of scour depth.

Conclusion

A model for scour depth as a function of periodic flow parameters has been developed by relating the shear stress results of CFD simulations to an empirical relationship derived from experiments. A strong trend was established for a canonical system with a large amount of experimental data available. This formulation was then expanded to incorporate local turbulence levels, which are a known driver of scour.

The resulting model was compared with experiments conducted with sand in a wave flume. A comparison with experimental data showed good results. In some cases, the local scour depth is well-predicted. On other cases, where local scour depth is not well-predicted, the extents of the scour area around the device predicted by the CFD simulation match fairly well with the experimental results.

Based on this initial analysis, the method developed in this study represents a feasible engineering method for predicting scour beneath an arbitrary body in waves. Note that scour is a fundamentally nonlinear process: the flow field redistributes sediment, which in turn changes the flow field. Thus the method considered in this study, which does not allow for deformation of the floor, is a linear approximation of this phenomenon. Future work should look at a wider range of wave conditions and consider a variety of devices/bodies.

III. Numerical Modeling SubReport (M3)

Objective

The following Computational Fluid Dynamics (CFD) analysis is in support of M3 Wave's ongoing development of subsurface wave energy devices (WEC). Simulations correspond to the 2017 physical testing at O.H. Hinsdale wave laboratory in Corvallis Oregon, focused on the wave-induced sediment scour associated with seafloor or near-seafloor based WECs. A fundamental goal of the Hinsdale experiment was the development of a CFD-based methodology for the practical prediction of scour to serve as a potential alternative to physical testing.

The greatest challenge in such development work was that the prediction of equilibrium seabed morphology would need to be based on fixed-bed CFD simulations. Ideally, the use of a coupled morphology model would allow for the interdependency of fluid patterns and bathymetry changes as the simulation progresses. While there are some early examples of coupled morphology models in the literature, these are very computationally intensive, with runs times on the order of weeks or months. A more practical approach was deemed necessary. The approach taken here was to leverage empirical scour formulae designed for simplistic structures and apply them to more complex structures utilizing fixed-bed CFD simulation techniques.

Numerical Model

The numerical model was developed using OpenFOAM, open source software for CFD ("OpenFOAM-dev" 2017). OpenFOAM offers a 3D solution to a system of equations describing mass and momentum conservation within a finely meshed computational domain. The pimpleFOAM solver used for this analysis is a single-phase solver specific to incompressible, immiscible, and isothermal fluids. Turbulence was estimated using the standard k-epsilon model. The CFD simulations represented full-scale physical dynamics corresponding to the experimental setup for the Hinsdale large wave flume. The dimensions of the CFD domain were 16m (length) x 3.6m (width) x 2 m (depth), representing the subsurface test volume containing the prototype structure and near-structure region. High resolution around the prototype was accomplished through graduated grid refinement. The 5.4m x 2.2m x 1.2m region of greatest refinement, indicated in yellow in figure 7, consisted of cells no more than 5cm³ in volume. Subsequent refinement via the snappyHexMesh utility was applied to finely integrate the structural details.

As dictated by test conditions 1-4, weakly nonlinear wave theory (second and third order Stokes expansions as seen the Le Méhauté diagram, figure 8) for intermediate depths were prescribed for top, right and left boundaries. The side and bottom boundaries were treated as symmetry planes. The bottom boundary and device surface were treated as fixed walls utilizing wall function boundary conditions suitable for the k-epsilon turbulence model.

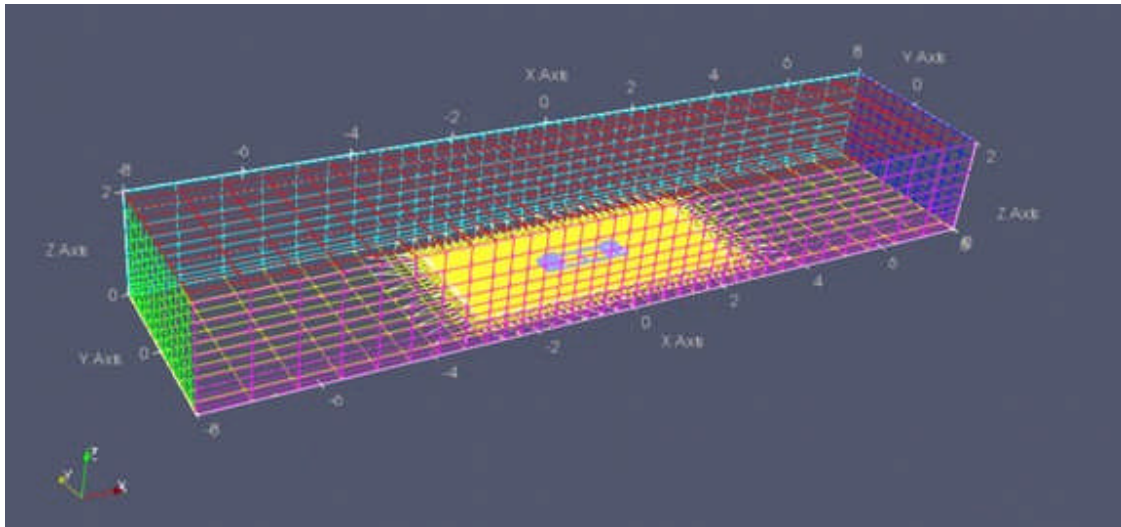


FIGURE 7. Cfd domain illustrating device placement and mesh refinement.

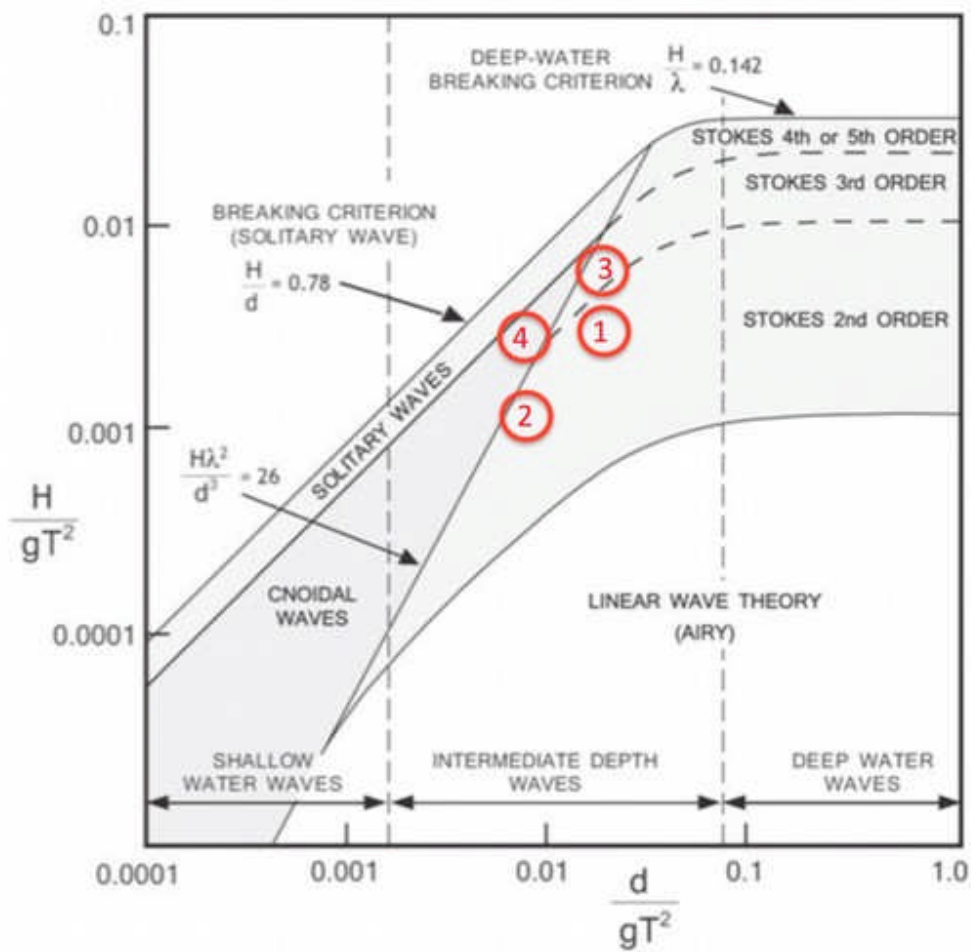


Figure 8. Le méhauté diagram (1976), with the four wave condition test cases indicated with red circles.

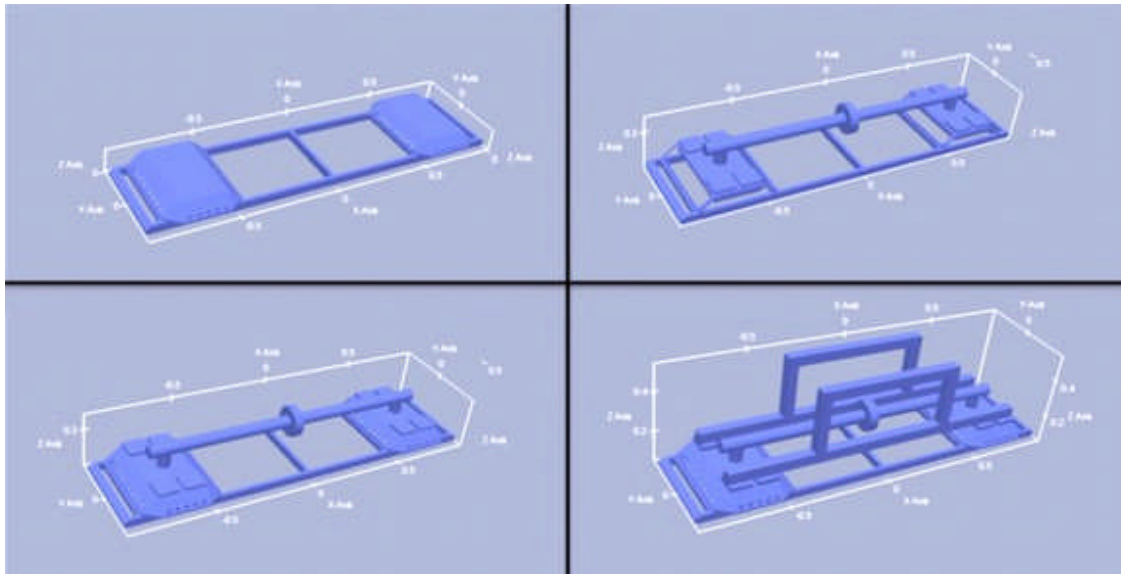


Figure 9. Apex representations used in cfd analysis. Clockwise from top left : “sleek”, “skeleton”, “apex with lift-frame”, and “default”.

Utilizing CFD Simulations to Predict Scour

Scour and accretion under waves are complex physical processes with many competing transport mechanisms. Empirical formulae exist for some very simple geometries, largely derived from studies specific to vertical piles and horizontal pipelines under waves. With the 2014 deployment data serving as a basis, the most analogous empirical model for APEX is the horizontal pipeline. The key flow features associated with three-dimensional pipeline scour are tunnel erosion, lee wake flow, and front-sided vortices caused by adverse pressure gradients. In order to better capture similar flow patterns for the flat-bed CFD treatments, the device representations were placed at a slightly elevated position (1 cm above the floor) within the domain to allow for flow streaming beneath device cross-members.

Empirical estimates for pipeline scour express maximum scour depth as a function of Keulegan-Carpenter Number ($KC = UT/D$), where D is the pipe diameter. The KC number is the main predictor of shedding vortices and so also the onset of net scour. At small KC values, the mean orbital motion of water particles is small relative to the width of the structure and flow separation is unlikely. For larger KC values, the stroke of the motion is long enough to generate flow separation. The challenge in this case is to extrapolate the 2D horizontal pipe scour methodology, which results in a bulk measurement (maximum depth), to a 3D scour “footprint” for more complex 3D structures like APEX.

Theoretical Basis of CFD-Based Scour Predictions

The CFD scour footprint was achieved with an effective KC map that was generated from the CFD simulation using bed shear stress output. Bed shear is related to scour in that areas of high shear

stress correspond to areas of scour, yet shear stress magnitudes do not fully correlate to scour magnitudes. Scour mapping is complicated by sediment redistribution and backfilling, processes better linked with turbulent flow patterns than with shear stress. Thus, the results were scaled using a mapping of turbulent kinetic energy (TKE) in effort to amplify scour predictions in areas directly under turbulent flow features. The final scour mapping was then tuned for each wave condition using a separate pipeline simulation for each wave condition. By utilizing the empirical relationships known for pipeline scour, each pipeline simulation allowed for a condition-dependent correlation between the CFD simulation and scour depth.

The CFD output cannot account for sediment accretion since sediment transport is not directly modeled. The redistribution of sediment was estimated post simulation, via series of simple transformations for qualitative purposes. The basis of the transformations came from a study of the experimental contours, concluding that sediment was typically diffused and shifted a short distance both forward and backward from the areas of scour. This strategy was applied independently to each transect of the CFD contour map, such that an accretion map could be derived from the scour map. Specifically, accretion transects were generated by applying three transformations to each scour transect: inversion, dilation, and translation. First the “missing” sediment was estimated by the inversion of the scour transect under the assumption of transport was confined to the near-structure region. Subsequently, the accretion was subjected to dilation (110%) to represent axial dispersion, followed by half-magnitude translations forward and backward (+/- 24cm) to represent bedload transport. All transformations were applied along the axis of wave propagation only. The final contour consisted of the sum of the accretion mapping and the scour mapping, with depths uniformly scaled to conserve the maximum scour depth as originally predicted.

Scour Model Validation

The group of physical testing labeled “APEX1” was used for model validation. In this test group, the APEX prototype, configured with the long axis oriented with wave propagation (0° orientation), was tested for all four wave conditions. The CFD simulations reproducing these runs were conducted using a sleek representation of APEX, as shown in the top, left pane of figure 9.

Resulting bathymetry contours are given in figures 10-13. For the following figures, the three contours on the left represent the measure net scan (top), the CFD output (middle), and the CFD output including sediment redistribution as estimated by the transformation algorithm described previously. The two panels on the right side represent an alternative view of the comparisons. Specifically, centerline transects of the measured scans are compared with transects of the CFD predictions: CFD without redistribution (top) and CFD with redistribution (bottom).

Notes for “A. Model Validation Runs”

The CFD-based model captured the general scour footprint across all wave conditions. For lighter wave conditions (figures 10 and 11), scour magnitude and lateral spread was in good qualitative agreement with measured net scans. However, at stronger wave conditions (figures 12 and 13), the model both under predicted the depths by approximately a factor of 2 and the lateral extent of scoured seabed.

The poor model performance for these strong wave environments was attributed to the idealized CFD representation of APEX. It was hypothesized that a truer representation one that included the orifice plate and attending support framework, would generate greater turbulence, and in turn

amplify the scour hotspots. This higher fidelity representation was generated and labeled “APEX default” in the bottom, left panel of figures 14.

Experimental contours showed asymmetry in the scour patterns for Wave 3 (Figure 15) and 4 conditions. This could be attributed to the due the nonlinear wave conditions inherent in the relatively shallow large wave flume. Some asymmetry, although less severe, was also noted in the simulations for wave conditions 3 and 4.

The validation cases were rerun using APEX (default). Contrary to expectation, the increase in turbulence generated by the fluid interactions with the orifice plate and attending structure did not generally amplify scour prediction. Instead, the added turbulence created a more diffuse flow environment that evened out hotspots.

Scaling the scour contour by a factor of 2 improved results as can be seen in figure 16. However, even with this scaling, the lateral spread of the scour footprint was not fully captured by the model.

Notes for “B. Effects of Geometry”

The addition of the orifice plate and attending support structure in the CFD representation of APEX led to slightly lower scour predictions for Wave 1 conditions, but more notably for Wave 3 conditions.

The subsequent addition of the lift frame structure did not produce further changes for Wave 1 and Wave 3 simulations. The major support beams within the lift frame were aligned with the principal flow, and had little affect on the simulation results.

The CFD scour predictions for the skeleton version of APEX showed good agreement with measured net scans for Wave 3 conditions. The skeleton structure more closely resembles a series of horizontal pipes, which fits well with the theoretical basis of the model.

It seems the added complexity of the default version of APEX is contributing to an important shift in sediment transport at stronger flow conditions. The model in its present mode, does not seem to be sensitive to this shift.

Notes for “C. Effects of Elevation”

The default version of APEX was simulated at 3 elevations (0cm, 5cm, 15cm) for Wave 1 conditions and compared to measured net scans.

In all cases, scour predictions agreed well in magnitude with measured data. Although in the elevated cases, simulated contours showed a slightly stronger pattern than was seen experimentally. 15cm was the height of the caisson. The top of the orifice crossbar was at 25cm. So an elevation of 15cm represents no more that one “APEX diameter”.

Note that the APEX is configured at 1cm above the floor in all “0cm” simulations to allow for streaming flow beneath cross-members.

Notes for: “D. Effects of Orientation”

Reasonable agreement with measured data was noted for 30 degree orientation for Wave 1 conditions.

Interestingly, there was generally lighter scour measured for the 60 degree orientation than was measured for the 30 degree orientation. This was not supported by the simulated contours.

With regard to the 60 degree orientation, model predictions showed a dominant scour pattern under the axial support members. This seemed less obvious in the measured contour, perhaps because the full length of APEX was not captured experimentally.

Model Validation Runs

- Waves 1-4, APEX (sleek, 0cm, 0°)

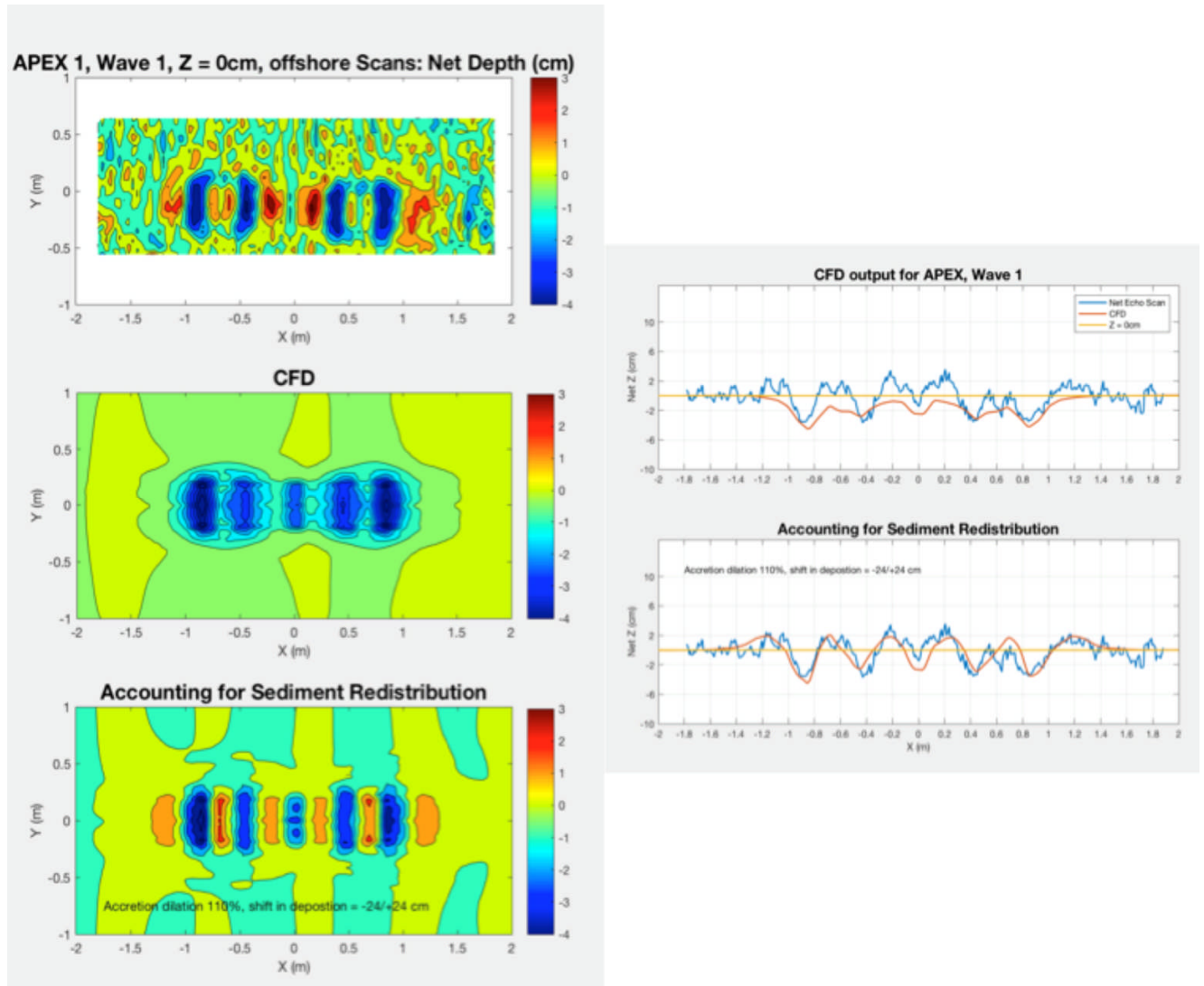


Figure 10. Wave 1 conditions. Cfd simulation of apex (sleek), raised 0cm and oriented at 0 degrees.

Right side graphs show comparison/correlation of CFD predictions (red line) and sonar scan slice of sediment (blue). In lower right graph, CFD model accounts for sediment redistribution.

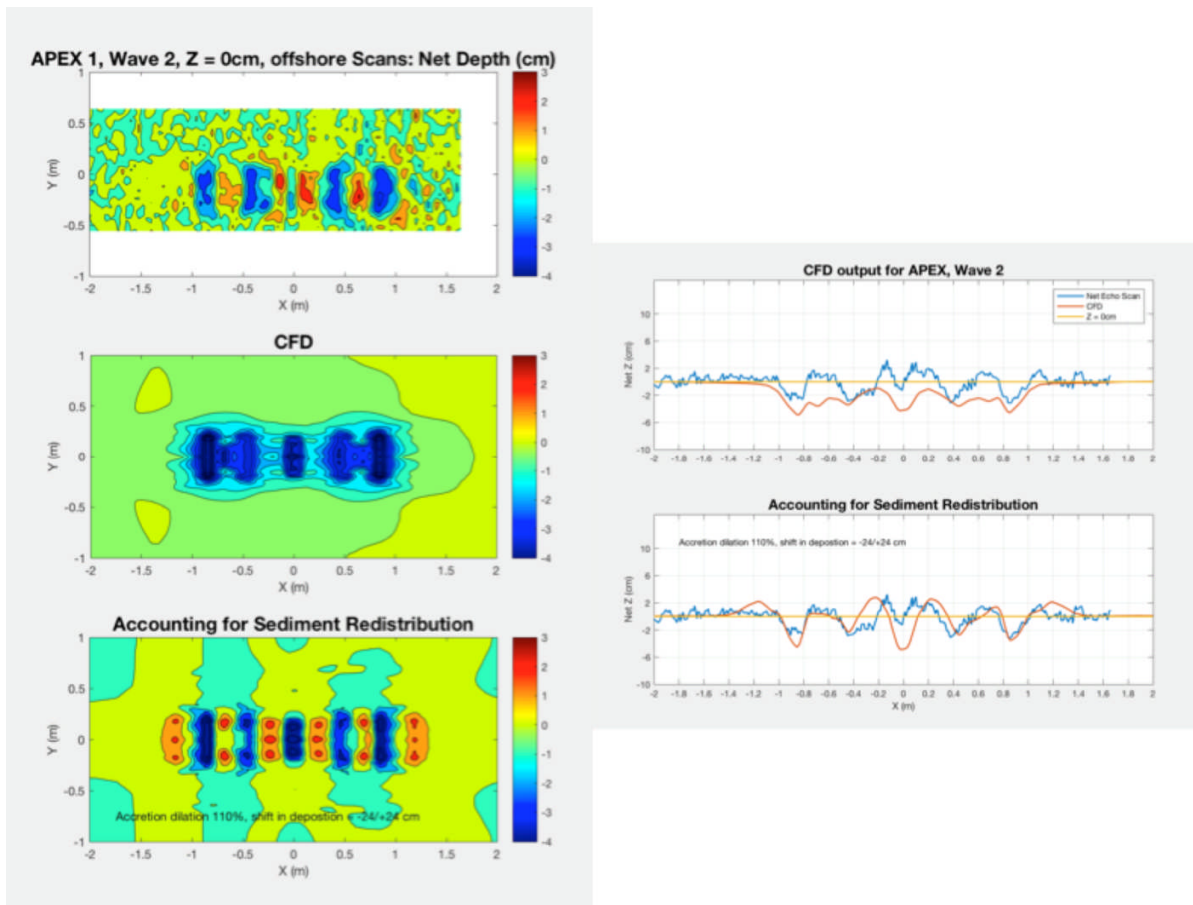


Figure 11. Wave 2 conditions. Cfd simulation of apex (sleek), raised 0cm and oriented at 0 degrees.

Right side graphs show comparison/correlation of CFD predictions (red line) and sonar scan slice of sediment (blue). In lower right graph, CFD model accounts for sediment redistribution.

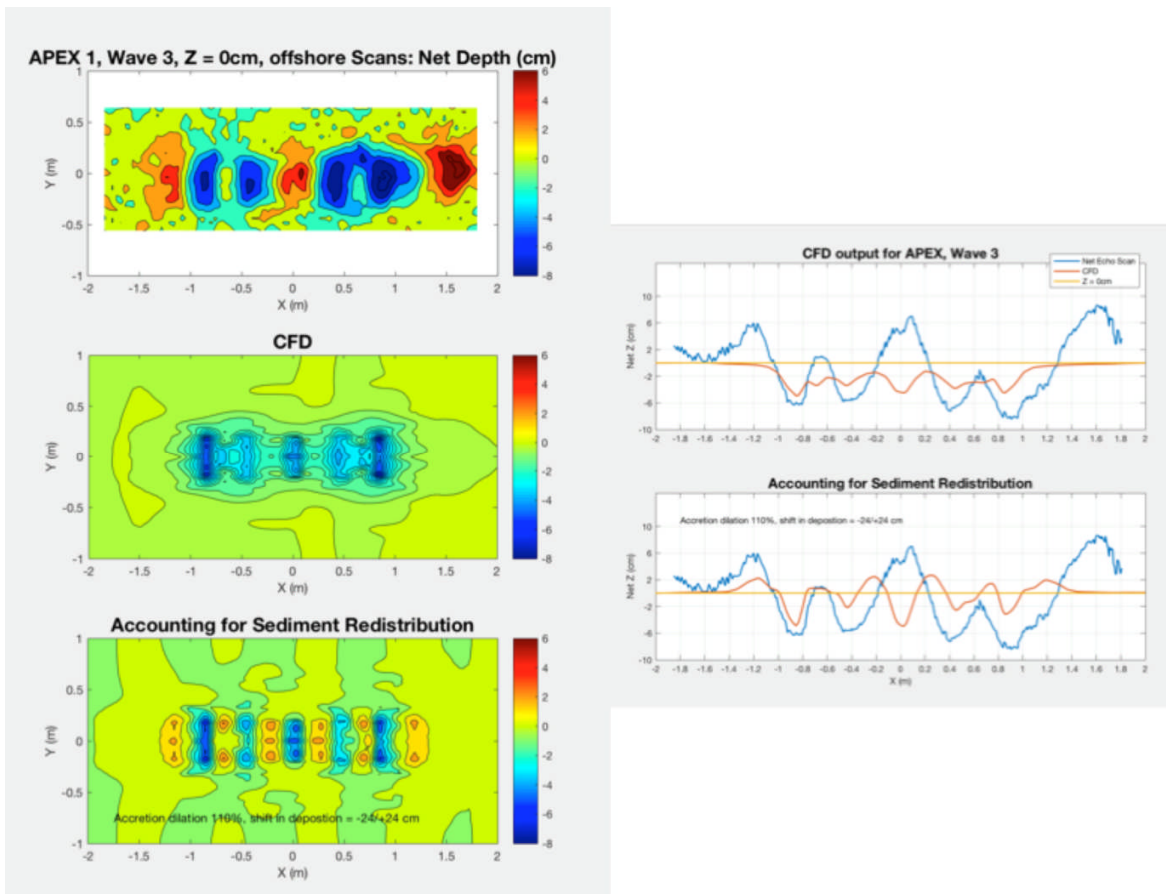


Figure 12. Wave 3 conditions. Cfd simulation of apex (sleek), raised 0cm and oriented at 0 degrees.

Right side graphs show comparison/correlation of CFD predictions (red line) and sonar scan slice of sediment (blue). In lower right graph, CFD model accounts for sediment redistribution.

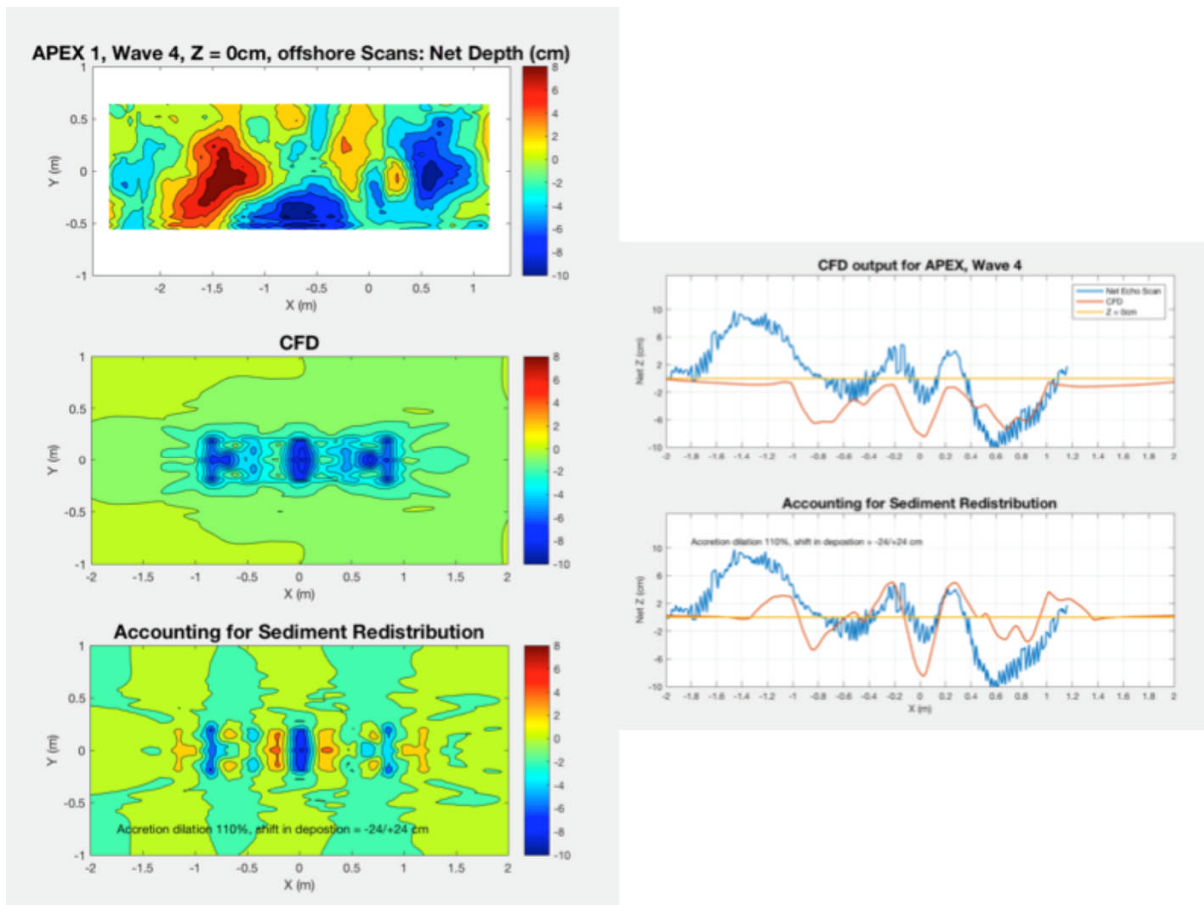


Figure 13. Wave 4 conditions. Cfd simulation of apex (sleek), raised 0cm and oriented at 0 degrees. Note in top left pane that wave-induced shifting of device away from centerline orientation occurred during experimental test.

Right side graphs show comparison/correlation of CFD predictions (red line) and sonar scan slice of sediment (blue). In lower right graph, CFD model accounts for sediment redistribution.

- Waves 1 and 3 (APEX default, 0cm, 0°)

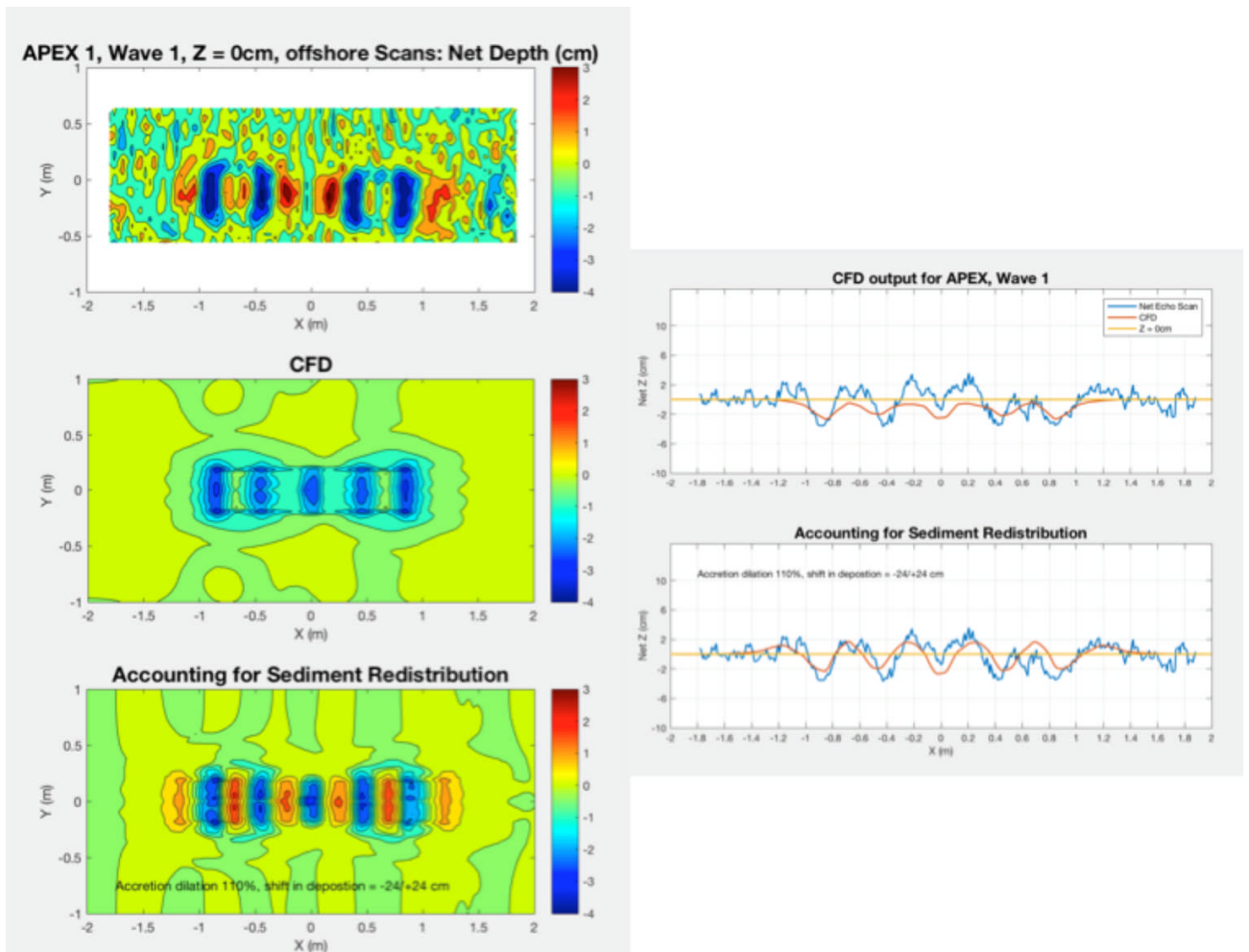


Figure 14. Wave 1 conditions. Cfd simulation of apex (default), raised 0cm and oriented at 0 degrees.

Right side graphs show comparison/correlation of CFD predictions (red line) and sonar scan slice of sediment (blue). In lower right graph, CFD model accounts for sediment redistribution.

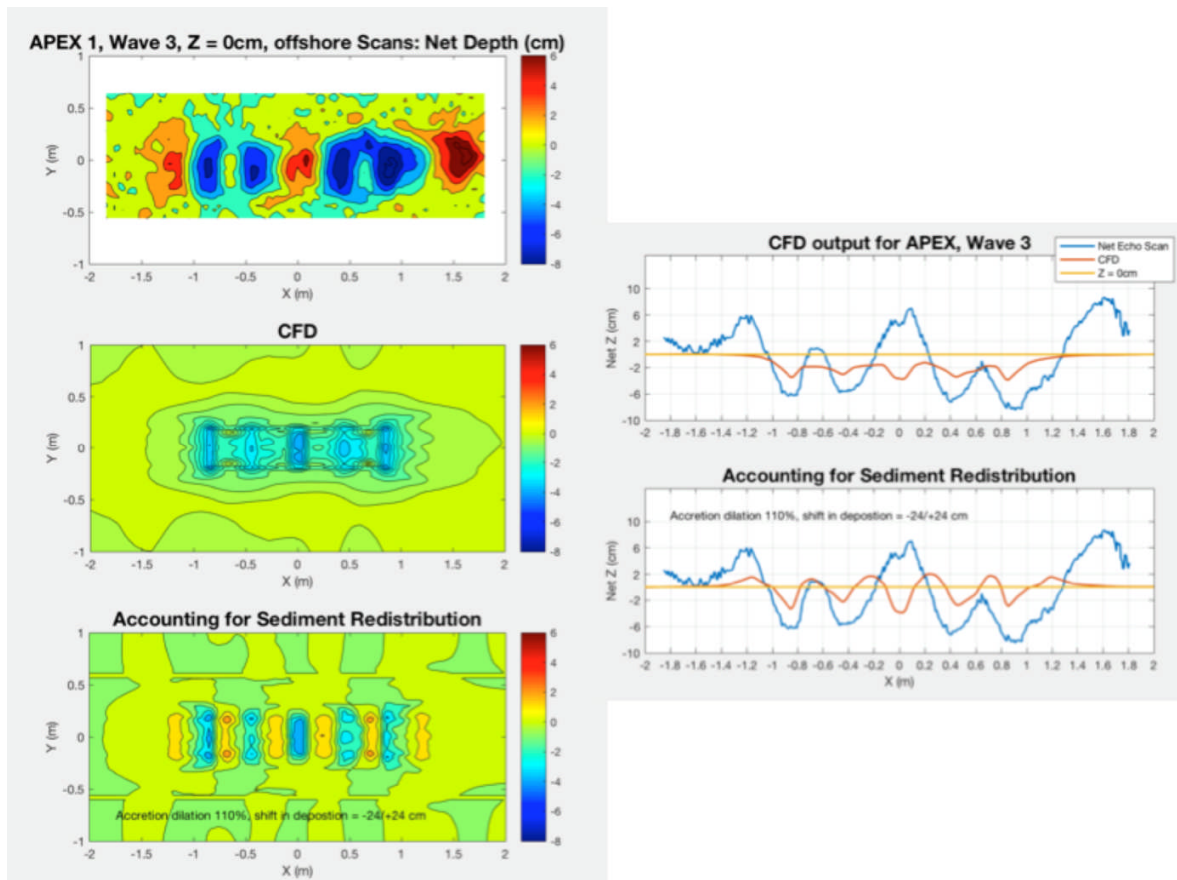


Figure 15. Wave 3 conditions. Apex (default version).

Right side graphs show comparison/correlation of CFD predictions (red line) and sonar scan slice of sediment (blue). In lower right graph, CFD model accounts for sediment redistribution.

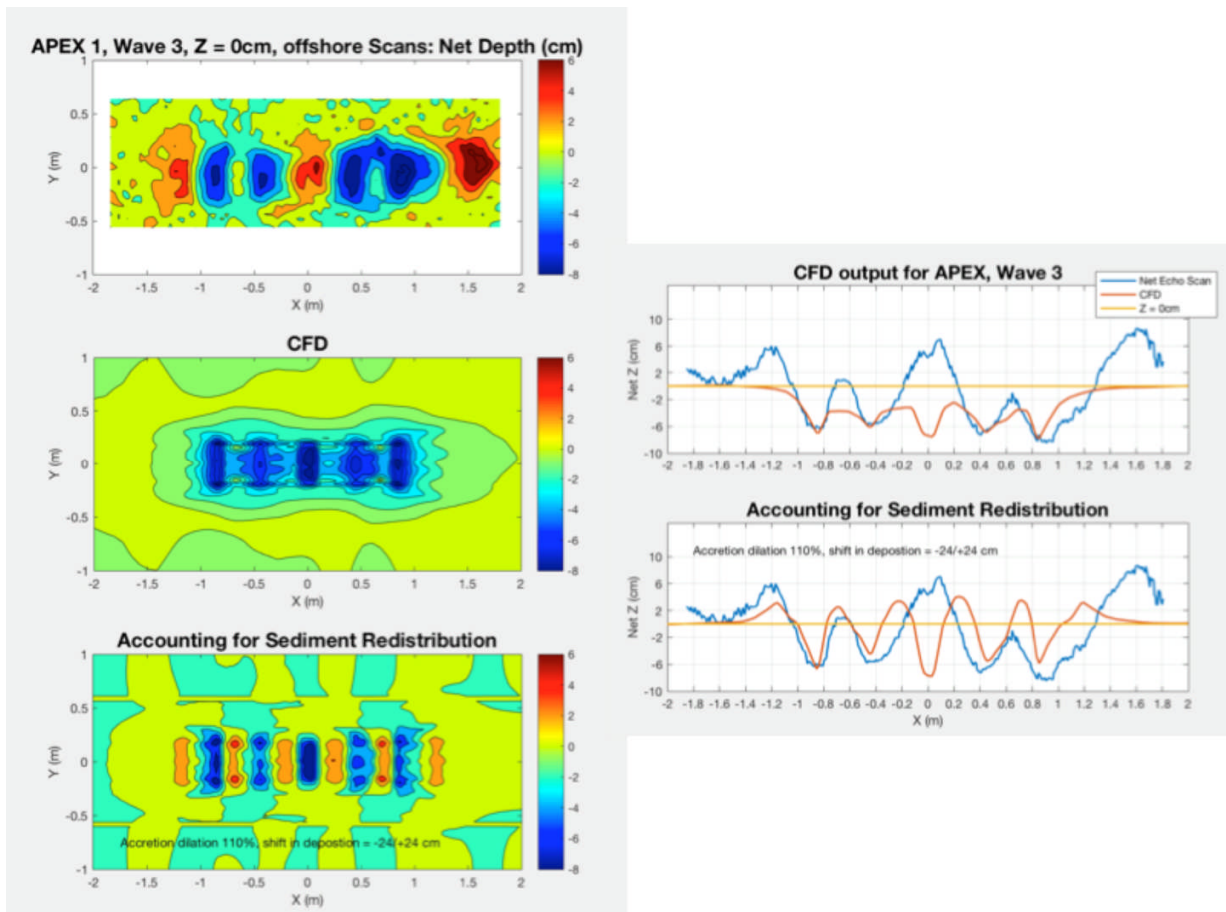


Figure 16. Wave 3 conditions. Cfd simulation of apex (default), raised 0cm and oriented at 0 degrees. Cfd results scaled up by a factor of 2.

Right side graphs show comparison/correlation of CFD predictions (red line) and sonar scan slice of sediment (blue). In lower right graph, CFD model accounts for sediment redistribution.

Effects of Geometry

- Comparison of APEX with lift frame (left) and APEX default version (right), Wave 3 conditions, 0cm, 0°

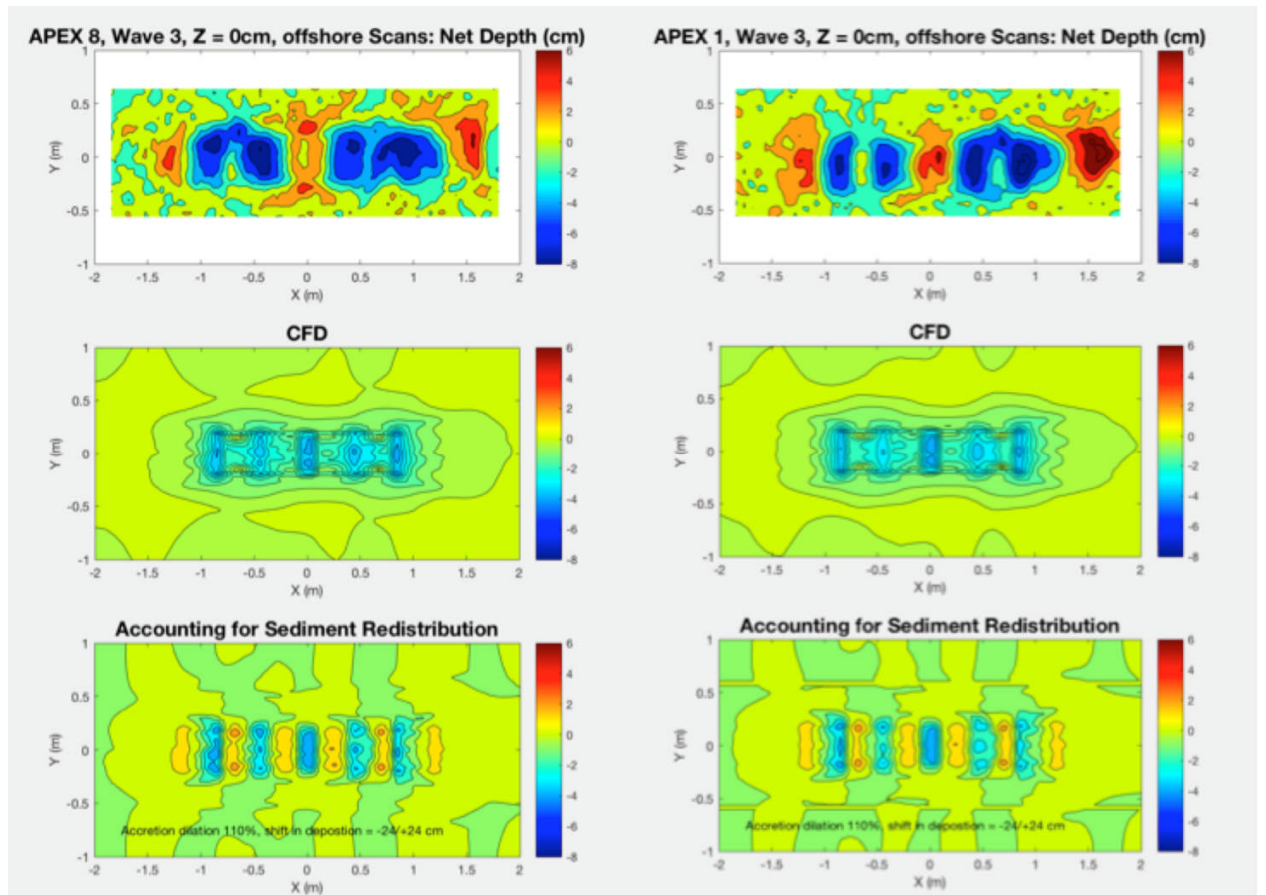


Figure 17. Wave 3 conditions. Left panels : measured data vs cfd simulation of apex (lift frame). Right panels : measured data vs cfd simulation of apex (default). For both simulations, device raised 0cm and oriented at 0 degrees.

Although the lift frame was required for testing involving elevating the device off the floor (see test section), there was concern that the lift structure might interact and change the sediment transport behavior. This series of simulations and runs were conducted to verify that the added structure would not affect sediment performance. The team concluded that the lift structure had no discernible impact on sediment transport when testing the worst-case scenario- default device sitting at elevation 0cm.

- Comparison of Skeleton (left) and APEX default version (right), Waves 1 and 3, 0cm, 0°

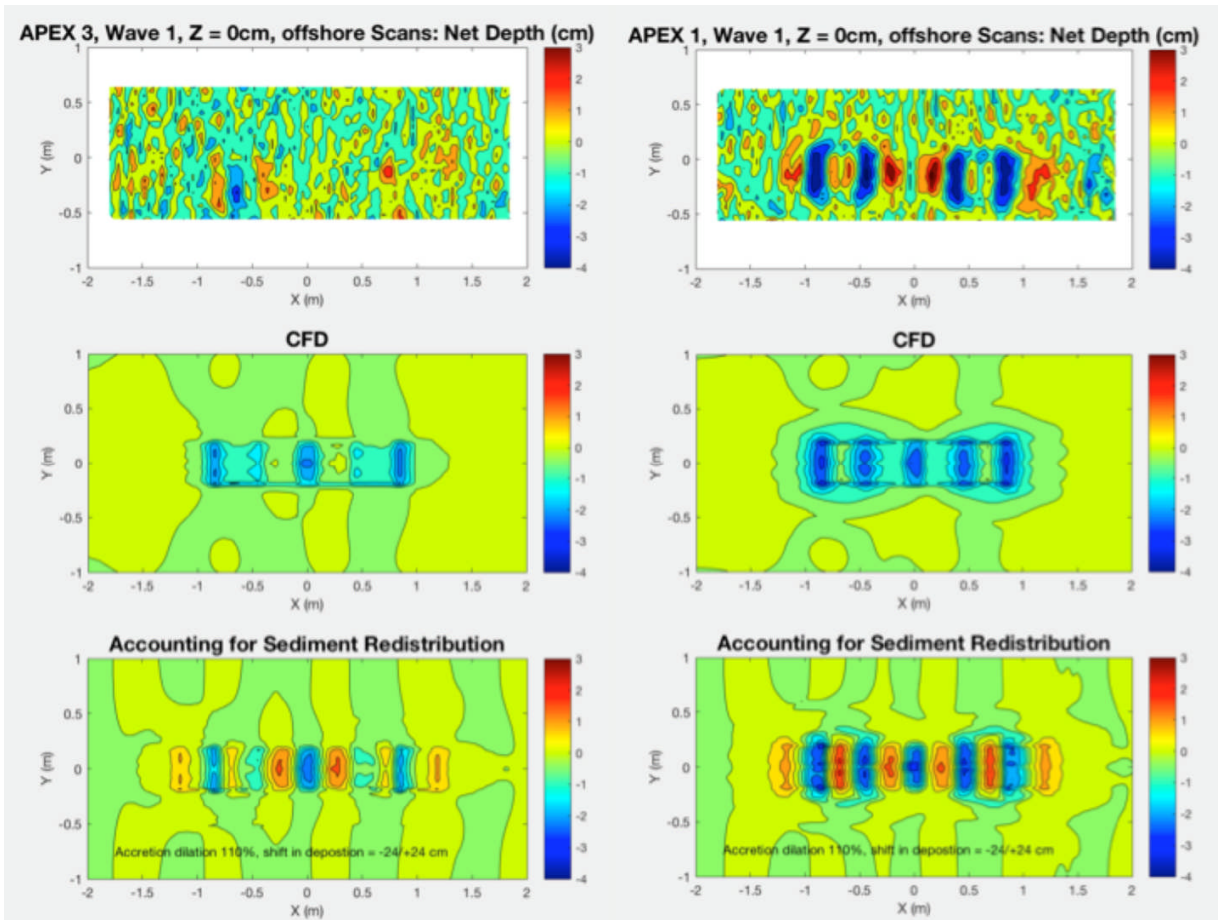


Figure 18. Wave 1 conditions. Left panels : measured data vs cfd simulation of skeleton. Right panels : measured data vs cfd simulation of apex (default). For both simulations, device raised 0cm and oriented at 0 degrees.

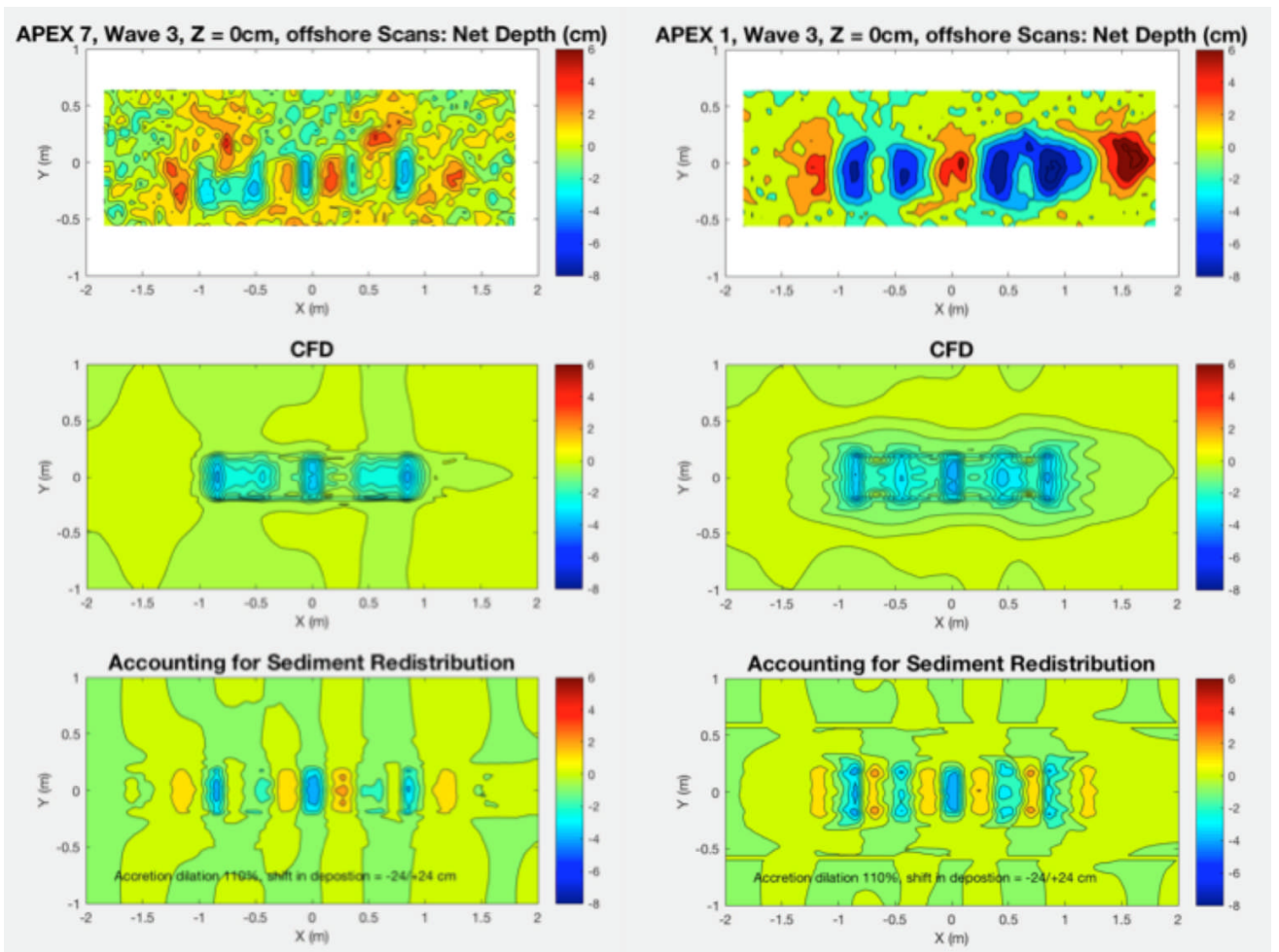


Figure 19. Wave 3 conditions. Left panels : measured data vs cfd simulation of skeleton. Right panels : measured data vs cfd simulation of apex (default). For both simulations, device raised 0cm and oriented at 0 degrees.

C. Effects of elevation

- Comparison measured vs model predictions for elevations of 0cm, 7cm, and 15cm.
APEX with lift frame, Wave 1 conditions, 0°

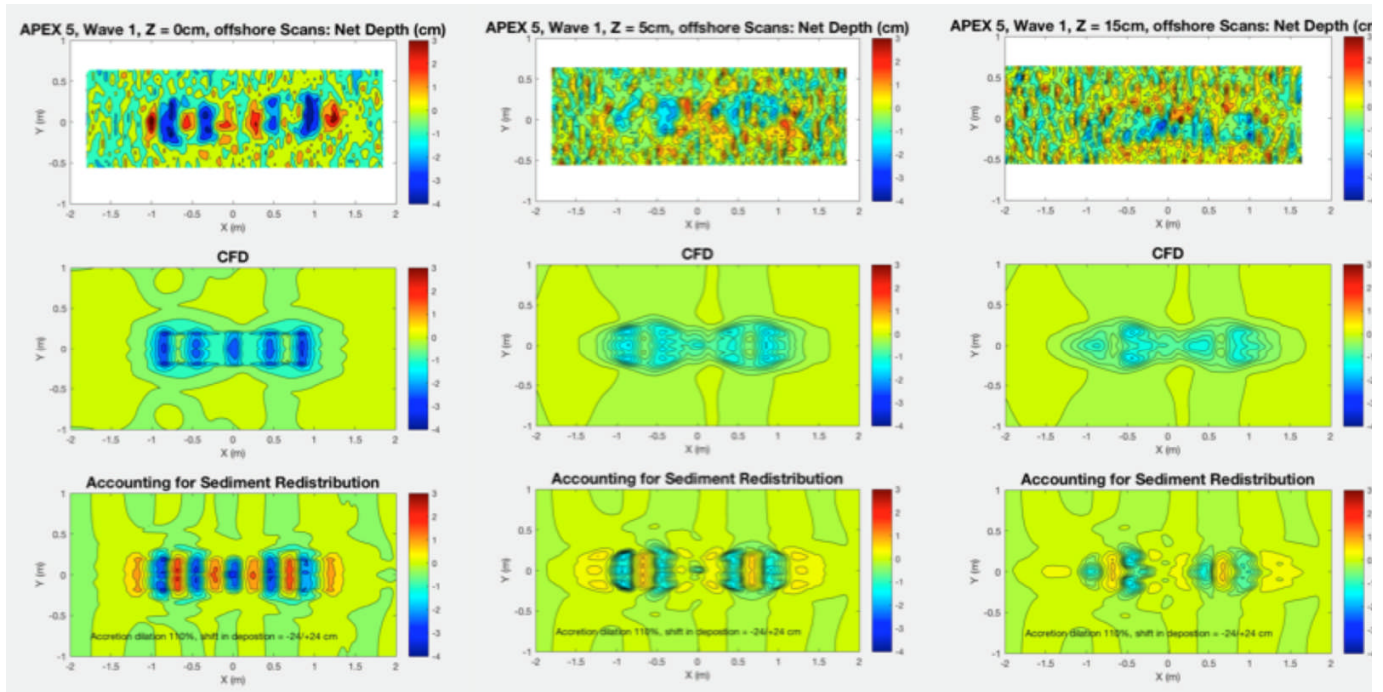


Figure 20. Wave 1 conditions. Left panels : measured data vs cfd simulation of apex (default). Center panels : measured data vs cfd simulation of apex (with lift frame) raised 7cm. Right panels : measured data vs cfd simulation of apex (with lift frame) raised 15cm.

D. Effects of Orientation

- Comparison measured vs model predictions for 0, 30o, and 60o orientations. APEX (default), Wave 1 conditions, raised 0cm

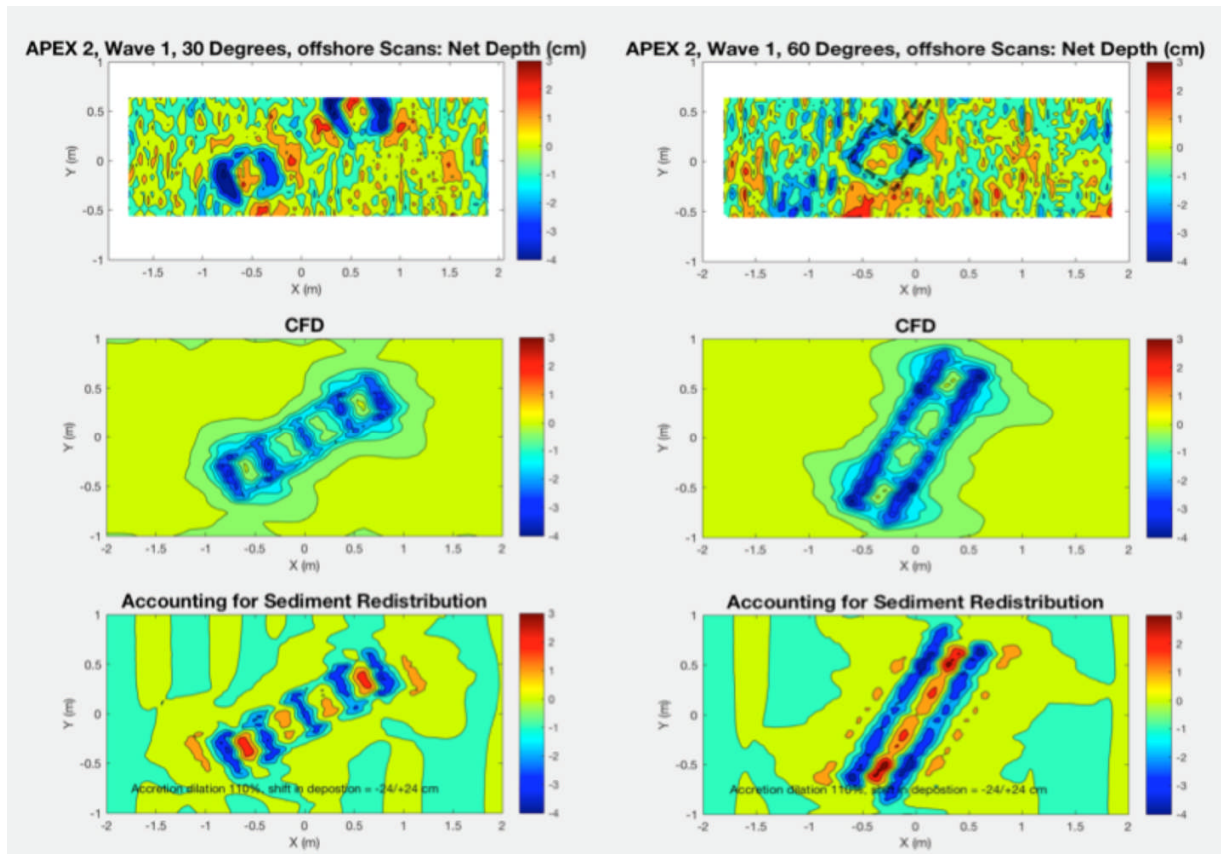


Figure 21. Wave 1 conditions. Left panels : measured data vs cfd simulation of apex (default) raised 0cm, 30 degrees. Right panels : measured data vs cfd simulation of apex (default) raised 0cm, 60 degrees.

Analysis

Let us consider the amalgam of results from each of the four preceding sections, including experimental scour investigations and numerical scour predictions.

In terms of understanding what aspects of the WEC lead to particularly poor scour performance, the WAMIT results are particularly insightful, especially when coupled with direct observation of sand particle motion. We now know that small gaps in the original design were leading to local fluid acceleration, and this can be easily remedied for future designs. We also learned that bag actuation / motion (during WEC operation) is not a significant factor relating to the fluid flow under the caissons. This was thought to be a significant mechanism relating to scour, and can now be deemphasized.

Regarding fidelity of testing, in particular with device elevation, we learned something about the lift frame method. We find with both lab testing, and CFD scour prediction, that the lift frame did not

significantly affect the scour/accretion results. It is satisfying that the numerical results match up with the empirical.

Elevation testing produced well-matched results between CFD and empirical testing. It was well known that elevating the WEC sufficiently far away from the seabed would eliminate scour. But now, we have a tool that allows us to make design and deployment trade-offs, where we can adequately predict scour performance at any arbitrary WEC elevation. A variety of elevations were tested to understand how scour reduces with device elevation. Successful mitigation of sediment scour occurred at a surprisingly low elevation- mere centimeters off the bottom.

In terms of WEC caisson design, all results are consistent in showing that the skeleton (minimalistic) caisson design is superior for scour and accretion. Both lab work and numerical work show that caisson orientation relative to incoming wave direction matters—although, the two efforts show opposite trends. It is unclear as to why the CFD-based scour does not trend the same as the empirical scour based on WEC orientation. Regardless, these results suggest that a more optimum, minimized caisson shape has the ability to measurably reduce local scour. However, in the laboratory experiments, we observed that the skeleton caisson (as configured) did not adequately protect the bags. This presents a design trade-off that may need to be further explored: is there an optimum in terms of caisson design which reduces scour (and associated device deployment longevity) and maintains adequate protection of the bags. Of course, there are aspects of bag design which will factor into this trade-off.

While it wasn't explicitly modeled, the suction pile deployment at 1:5 did mimic the CFD scour predictions at 5cm and 20cm elevation. Since this deployment method is viable for large, ocean deployed devices in some locations, it is encouraging that it provides a useful knob for reducing scour related problems.

Conclusions

A model for scour depth as a function of periodic flow parameters has been developed by relating the shear stress results of CFD simulations to an empirical relationship derived from experiments. A strong trend was established for a canonical system with a large amount of experimental data available. This formulation was then expanded to incorporate local turbulence levels, which are a known driver of scour.

The resulting model was compared with experiments conducted with sand in a wave flume. A comparison with experimental data showed good results. In some cases, the local scour depth is well-predicted. On other cases, where local scour depth is not well-predicted, the extents of the scour area around the device predicted by the CFD simulation match fairly well with the experimental results.

Based on this initial analysis, the method developed in this study represents a feasible engineering method for predicting scour beneath an arbitrary body in waves. Note that scour is a fundamentally nonlinear process: the flow field redistributes sediment, which in turn changes the flow field. Thus the method considered in this study, which does not allow for deformation of the floor, is a linear approximation of this phenomenon. Future work should look at a wider range of wave conditions and consider a variety of devices/bodies.

IV. Experimental Lab Work (Empirical Testing)- Laboratory Experiments at 1:25 Scale

Introduction

Within the context of the current work, the 1:25 scale laboratory experiments are used as an initial touch point to validate that scour observed in the 2014 ocean deployment of a prototype, scaled APEX can be replicated in the lab. While we recognize that the scaling of the sand is poor (even though it is identical sand) such that the sand at 1:25 will behave like rocks, it would be encouraging if similar scour extent and locations were observed when compared to diver's footage in 2014. These 1:25 tests are intended to be qualitative, and will help us to develop a more refined plan for the 1:5 tests later.

Experimental Methods

Testing was performed in M3's wave flume in Salem, Oregon. The flume is 30 feet long, 3 feet wide, and 3 feet deep. A sediment region was created that extended the full width of the flume, was 5 feet long, and one inch deep. The full sand/sediment area was viewable through a plexiglass wall on one side of the flume. Waves were generated with a flap style wave maker. Water depth was set to 1:25 of the 2014 deployment depth (approximately 24 7/8"). The flap wave maker generated 1:25 scaled wave heights and wave lengths that mimic Oregon coast average waves, as described in table 3.

Wave	Description	H (in)	T (s)
A	Regime IV	3.1	2.6
B	Operating Condition	3.1	1.5
C	Storm	6.3	2.1

Table 3. Wave conditions tested at 1:25 in the M3 Wave flume.

1:25 scaled models of the "standard" APEX device, and the "skeleton" APEX device were 3D printed in nylon: overall WEC length 14.4", caisson width 3.8", and caisson length 2.4." The accurate 3D printed models included all gaps, holes and features that might influence fluid flow near the WEC. This turned out to be important later, as the numerical modeling showed dramatic fluid velocity increase near a gap between the caisson and the outer frame rail.

Oregon coast sand was raked smooth in the test area prior to each test. Then, the 3D model was placed on the sand, with a small weight on top of each caisson, prior to starting monochromatic waves. Waves were run for fifteen minutes, with continual observation. After wave completion, the small WEC was carefully lifted up, and set down beside the test area so that the WEC and its scour could be seen together. In some cases, a high intensity light was used to cast the scour into relief, and photos were taken. While the depth of scour was measured at several locations, the qualitative aspects of scour will be the focus of this section.

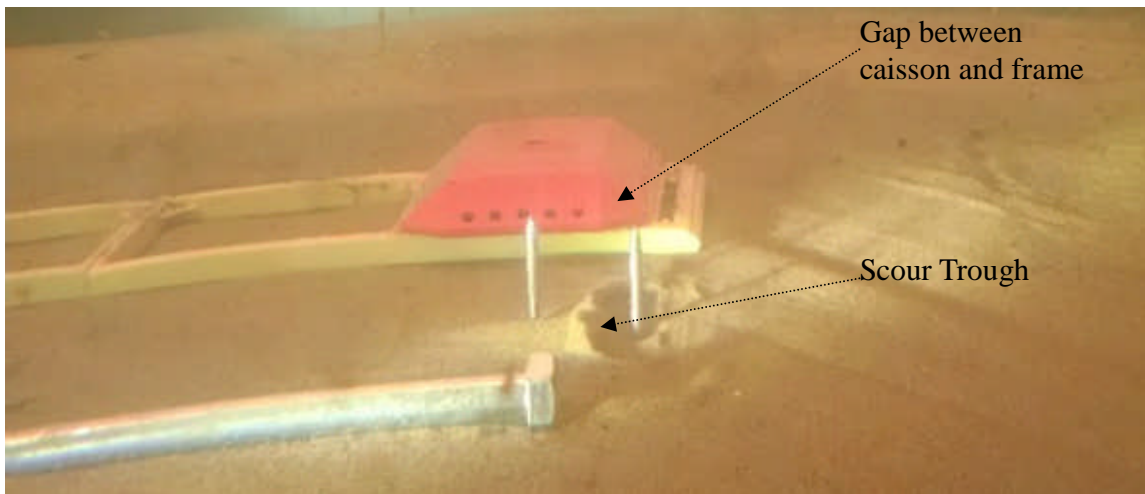


Figure 22. 1:25 standard APEX design. Model has been lifted and placed adjacent to scoured and accreted areas for illustrative purposes. Metal bolt and rods used for scale reference. This is after wave A “Regime IV” waves. A scour “trough” is seen at the right most vertical rod, which corresponds to scour under the right most gap in the WEC (seen between the red caisson and the yellow frame rail).

Results

During wave operation with the standard APEX design, local acceleration of water was evident at each end (fore and aft) of the WEC for all three wave conditions. This could be observed by seeing bits of sand moved locally, and after a while, an eroded area was apparent. With the WEC removed, it was then more apparent that scour was occurring under the caissons, and sand accretion was occurring near the central cross bar. Both of these behaviors were seen in the 2014 ocean deployment. Further, there was local buildup and removal in various places along the length of the longitudinal frame rails, and outboard of the fore and aft rails.



Figure 23. 1:25 standard APEX design on sand, behind scoured area. A scour trough can be seen at each end near the caisson to end rail gap. Sand build up at the central rail is also seen. This is after 15 minutes of wave A, Regime IV waves.

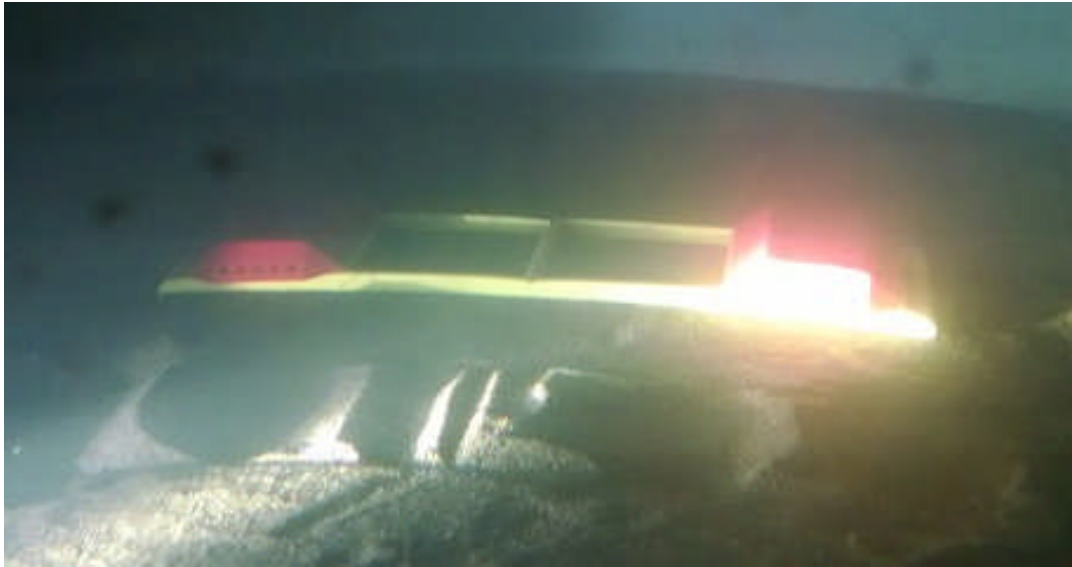


Figure 24. 1:25 standard APEX design on sand, behind scoured area. Large scoured areas are found under the caissons. This is after wave C, storm waves.

In contrast, when the skeleton caisson design was used, local acceleration was not observed for either wave A nor wave B (wave C was not tested), and significant scour was not observed under the WEC after removal.

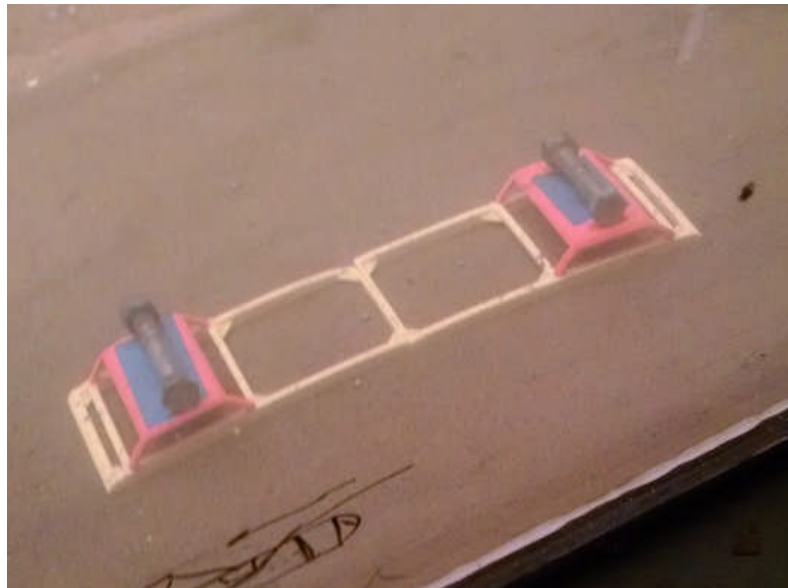


Figure 25. 1:25 skeleton caissons on APEX frame during testing in M3 wave flume.

Analysis / Conclusions

Qualitatively, we were able to show that a 1:25 scaled model of the original APEX could produce scour in locations and extent similar to the much larger, ocean deployed device. Further, we showed that under the same wave conditions, a minimalist caisson (aka “skeleton”) could make significant reduction in local scour. These results are encouraging, and suggest that the upcoming 1:5 scaled model testing will also be able to develop scour and accretion.

V. Experimental Lab Work (Empirical Testing)- Laboratory Experiments at 1:5 Scale

Introduction

Within the context of the current work, the 1:5 scale, Hinsdale wave laboratory experiments are used as the “larger scale” validation of two items: 1) scour observed in the 1:25 scaled tests; and 2) predicted results from numerical modeling. Scaling of the sand is better here than in the 1:25 tests, but is still not ideal. However, for consistency, we use Oregon coast sand with the same nominal composition and size distribution as the original 2014 deployment. These 1:5 tests are intended to be quantitative, and will be the most convincing evidence that the team can use (within this study) to attempt to validate the numerical scour models.

Experimental Methods

Testing was conducted at Oregon State University’s large wave flume at the Hinsdale Wave Research Laboratory during portions of July and August 2017. The large wave flume is equipped with a piston-type, hydraulic wave maker. It is 104m long, 3.7m wide, and for our testing, was prepared with a 0.5m deep layer of sand ($d_{50} \sim 0.2\text{mm}$), and used 2.7m of water depth. Versions of three M3 Wave prototypes were installed in turn (standard caisson, minimalist “skeleton” caisson, and a suction-pile deployed version). The WECs were installed at either 0 degrees to the tank axis, 30deg, or 60deg. The WECs could be mounted to a “lift frame” which allowed the WEC to be deployed at any arbitrary depth, thus allowing exploration of the effect of elevation upon scour. There were four, monochromatic wave conditions tested.

The wave conditions used in the 1:5 testing are scaled to the wave conditions experienced by APEX in the ocean in 2014, and are summarized in Table 4. Wave 1 represents typical 2014, deployment “operational” conditions (ocean scale (aka 1:1 scale): wave height, $H = 1.5\text{m}$, wave period, $T = 8\text{s}$, maximum orbital velocity at seabed, $U_m = 46\text{ cm/s}$). Wave 2 represents a subset of the 2014 deployment wave conditions where longer wave periods were observed, this is sometimes referred to as “regime IV” (Ocean scale: $H = 1.5\text{m}$, $T = 13\text{s}$, $U_m = 57\text{ cm/s}$). Wave 3 represents a local storm (one that might be seen during summer) conditions ($H = 3\text{m}$, $T = 8\text{s}$, $U_m = 91\text{cm/s}$). Wave 4 represents “winter” storm conditions ($H = 3\text{m}$, $T = 13\text{s}$, $U_m = 110\text{cm/s}$), which were not seen during the 2014 deployment, but were more typical of a winter storm at the deployment location.

wave	H (cm)	T (s)	U_m (cm/s)	KC ($D = 5\text{cm}$)	Representative conditions
1	30	3.6	21	15	2014 typical operation
2	30	5.8	25	30	2014 deployment, “regime IV”
3	60	3.6	41	29	local storm
4	60	5.8	45	57	winter storm

Table 4: Experimental Wave Conditions. U_m = maximum bottom velocity, $KC = U_m T/D$, mean-water level = 2.7m, grain size of sand estimated at 0.2 mm

Scour assessment was made using bathymetry scans, using a custom configuration of 2MHz, Seatek ultrasonic depth finding transducers (multiple transducer array, or MTA), and scans were taken at multiple stages during each test run. Resolution of the MTA has been previously reported as 1mm in the vertical direction, and 2cm in the horizontal (along the MTA axis) direction. Resolution along the wave flume axis is governed by a laser range finder which locates the position of the MTA relative to the flume, and is reportedly better than 1cm. The transducer arrays held eight individual transducers, set at 8cm from center to center of each transducer (figure 26). Transducers were interleaved to double the across tank scan resolution (figure 27). Transducers operated at 2MHz, and had a half-angle of 1.1 degrees, with the sensors roughly 20" above the sandy bottom.

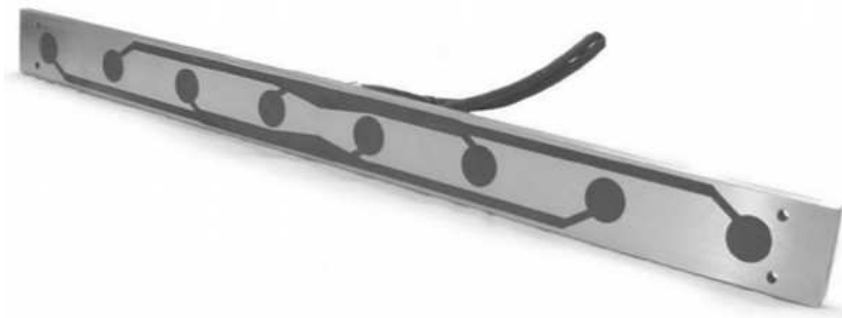


Figure 26. Bottom view of one of the Seatek, ultrasonic transducers that was used to measure sand elevation as part of scour evaluation.

a)



b)



c)

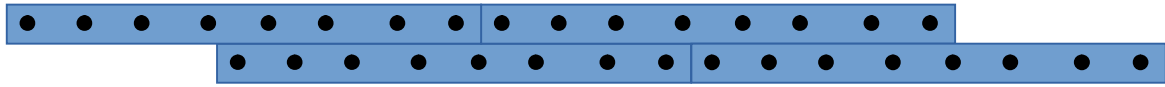
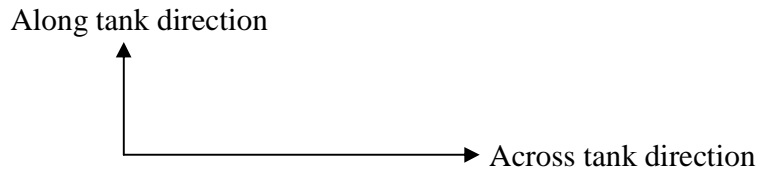


Figure 27. Schematic illustration (bottom view) of sonar transducer configurations. a) Showing a single array of eight transducers. b) Showing the typical configuration of the arrays, in a single line, with “default” across tank resolution. c) Showing the configuration used for bathymetry scans in this study, which effectively doubles the across tank resolution.

Pre-scans were taken of the sandy floor prior to testing and before the installation of the test structure. Post scans were taken after testing and removal of the test structure. The contours generated here represent net scans (differences between the pre-scans and post-scans). When possible, intermediate scans were also run with the test structure present, both before and after testing. These scans were useful in marking the location of the structure relative to the scour patterns. In between test conditions, the sand was manually raked, and then inspected with an ROV to determine if the sandy bottom had been adequately smoothed/flattened. The ROV typically made three transects along the tank axis. However, some pre-scans reveal that the initial floor condition was not ideally level prior to testing (e.g., wave 4). Minor irregularities in bathymetry would likely have little impact on results, as focus was given to net changes. Further, equilibrium scour is generally not strongly dependent on initial flow (or bed) conditions, but rather, on final flow conditions. Still, significant unevenness in initial bed conditions could potentially cause a tilted installation of the test-structure, affecting structure stability during the test run. This is a suspected cause of the wave-induced destabilization of APEX during the wave 4 testing.

In order to determine how many waves needed to be run in order to reach equilibrium scour conditions, we ran an initial set of tests with the standard caisson WEC with wave 1. This wave has the combination of least amplitude and shortest period, which suggests that it would reach equilibrium scour at least as late as the other wave conditions. In other words, waves with greater amplitude and longer periods are expected to disturb the seabed sooner/faster and develop equilibrium quicker. In this series of experiments, the sand was raked smooth, then wave 1 was run (with no WEC) for 10 minutes, developing regular sand ripples. The sand was imaged, then the WEC was set on the rippled, sandy bottom, and imaged. Then wave 1 was run for ten minutes, and the sand was imaged at the side of the WEC rail (see figures 28 and 29). Then, wave 1 was run for ten more minutes prior to reimaging. Ripples in the sand at the edge of the WEC rail developed within the first 10 minutes, and small areas of accretion/scour could be observed. This procedure was repeated until the accreted/scoured areas did not grow with successive waves. It was determined that 30minutes were required to ensure equilibrium sand accretion / scour.



Figure 28. A typical live image from the ROV controller, showing ripples developed in the sediment after running waves. From this view, scour and accretion could be assessed relative to the horizontal, grey frame rails.



Figure 29. Image of the sand build up at the frame rail during equilibrium testing. Image was taken via ROV.

The key WECs, shown in Figures 30-35, were 1/5 scale versions of the APEX prototype that had undergone the 2-week deployment in 2014. The “standard” caisson design WEC (see figure 30) has all structural dimensions Froude scaled by a factor of 5 down from the larger, 2014, ocean deployed version. The “skeleton” caisson design (see figure 31) started out as a standard caisson, but had nearly all of the sloped surfaces removed, thus minimizing the cross section of the caisson, when viewed by an incoming wave. This also means that the bags, which reside within the “enclosure” of the caisson, are more accessible to impinging waves.



Figure 30. Standard caisson design for APEX tested at Hinsdale. This caisson design matches that tested in the ocean in 2014. Also seen in the image are the frame (grey, below the caissons), and the oscillating air column, and tygon tubing air lines used to measure air flow within the device (verify operation of the WEC)



Figure 31. A stripped down version of the "skeleton" APEX device tested at Hinsdale. This WEC has the same frame as the standard WEC, but its caisson's have had most of the "sloped" surfaces removed, allowing water to flow through the caisson area / bag area more easily. Note, the air column is not present in this image.



Figure 32. The skeleton APEX being lowered into the flume, with the air column, bags, and tygon air column measuring lines in place.



Figure 33. The “lift frame is shown, suspended via its vertical screw. Note, there are levels on the frame for viewing via underwater camera and ROV during testing and deployment. There are also two ADVs mounted aft of the WEC: one is in line with the WEC, and one is outboard, to starboard.



Figure 34. Image of the standard caisson APEX design, mounted to the lift frame, for testing the WEC at various elevations off of the sandy bottom.



Figure 35. Image of the standard caisson WEC, with suction pilings for “pulling” the WEC down to any desired elevation from the sand.



Figure 36. The vacuum manifold system used to measure and apply suction to each of the suction piles during deployment of the “suction pile” WEC.

Results

Net bathymetry scans are shown alone, here, and in the numerical modeling section of this report, side by side with numerical modeling predictions of scour for the same waves. In general, we did find a range of scour and accretion depths/heights, and we did find a range of x-y scour extent. Comparison to numerical predictions will be discussed in another section. However, some generally observed empirical trends are presented here:

Influence of Wave Conditions

Wave condition (height and period) matters. As expected, bigger waves lead to more scour, and greater scour extent. For the same wave height, period appears to change the depth and extent of scour, viz comparing wave 1 and 2 data for the standard caisson design. See figures 37 and 38.

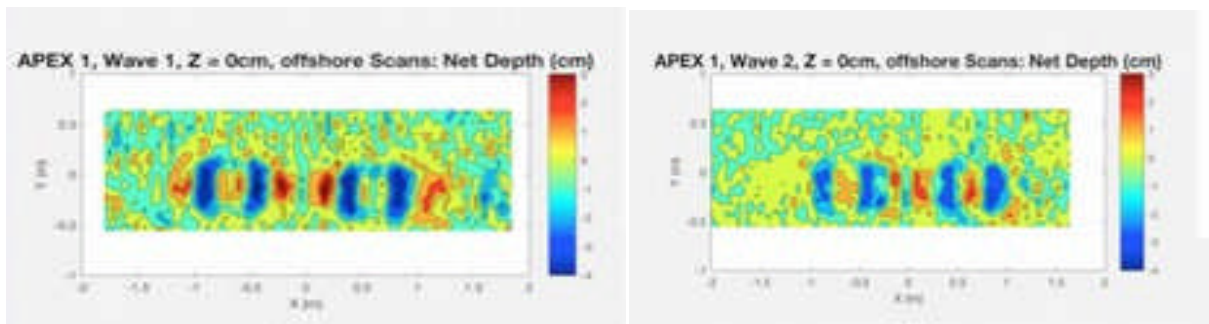


Figure 37. Net bathymetry comparison between wave 1 (left) and wave 2 (right) for the standard caisson WEC. Blue indicates scour while red indicates accretion.

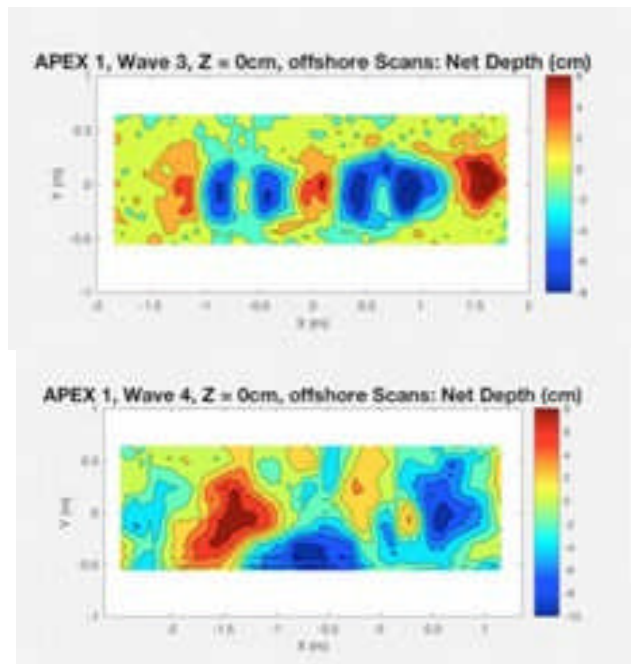


Figure 38. Net bathymetry comparison between wave 3 (left) and wave 4 (right) for the standard caisson WEC.

Influence of Caisson geometry.

Caisson shape/design matters. The standard caisson leads to dramatically increased scour for waves 1 and 3, when compared to the skeleton design. (see figures 39 and 40) However, while the skeleton caisson is very helpful for reducing scour, it does not protect the bags. During operation of wave 3 with the skeleton caisson, it was observed that the bags were not staying put, and were moving dramatically in the x-y plane (primarily in the surge direction). This type of motion would inevitably lead to bag failure, or bag-to-air column seal failure. Note, this large bag movement was not observed with wave 1 (skeleton design).

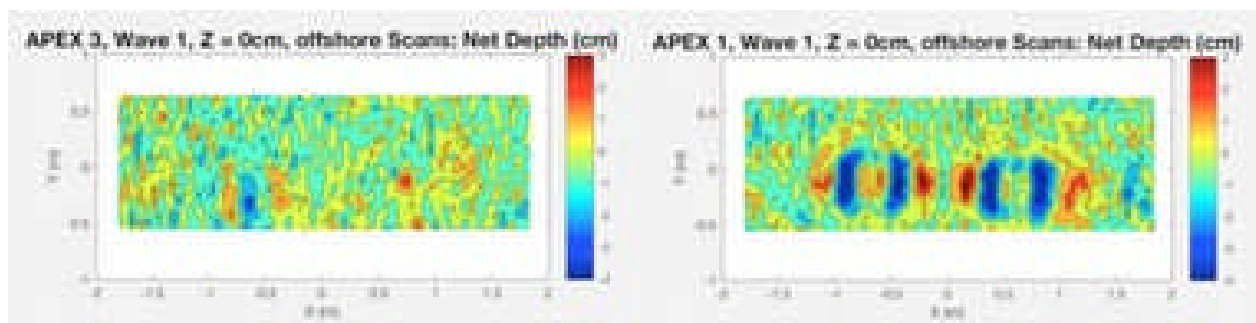


Figure 39. Net bathymetry scans comparing skeleton (left) and standard caisson (right) for wave 1.

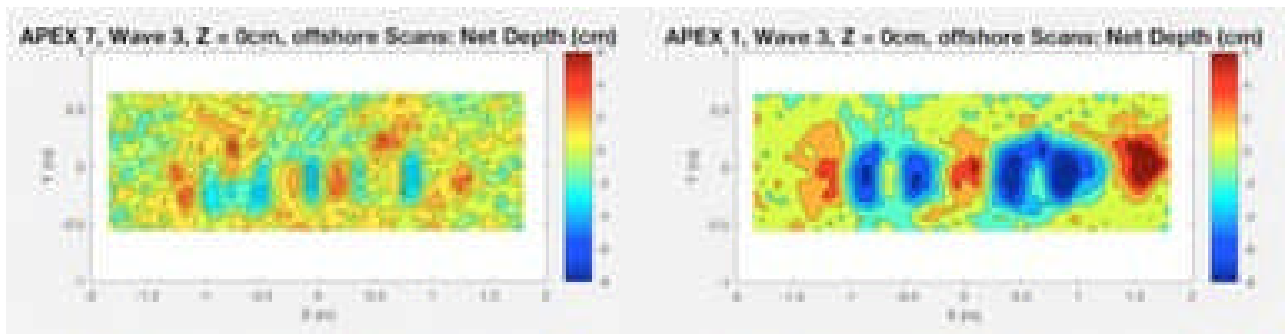


Figure 40. Net bathymetry scans comparing skeleton (left) and standard caisson (right) for wave 3.

Influence of elevation off bottom.

Elevation matters. Elevations of 0, 7 and 15cm were tested using the lift frame with the standard caisson WEC. The obviously scoured and accreted regions seen at 0cm elevation are not seen at either 7cm, nor 15cm elevation (see figure 41). However, at 7 and 15cm there is a hint of a non random scour in the same general configuration as the WEC. Regardless, we find that raising the WEC off of the seafloor by as little as 7cm can have a dramatic effect on reducing scour and accretion.

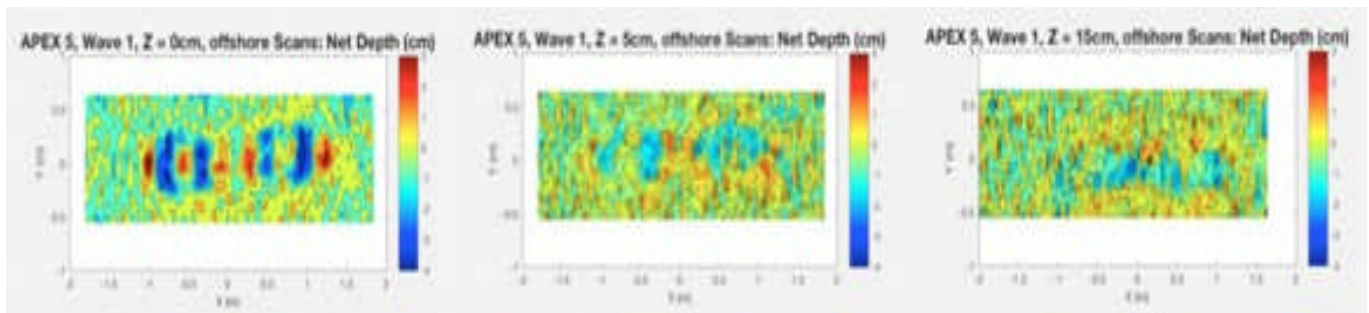


Figure 41. Net bathymetry scans comparing the standard caisson WEC at the sea floor (left), elevated using the lift frame by 7cm (middle), and by 15cm (right).

Influence of Device Orientation

Orientation to incoming waves matters. When comparing the standard caisson WEC aligned with the wave train, then rotated to 30 degrees, and 60 degrees, we find that scour generally decreases. It appears that the default caisson design promotes scour when aligned with the waves, and decreases scour when oriented further away from “aligned.” (see figure 42)

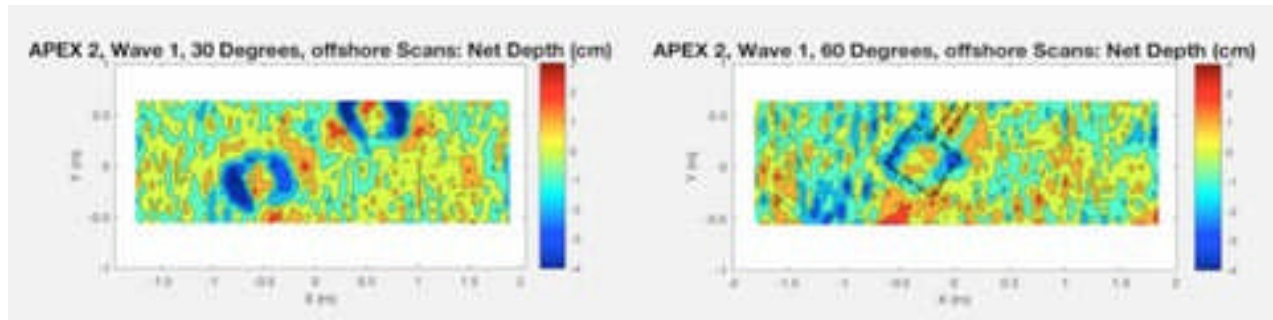


Figure 42. Bathymetry net scans comparing 30 degree orientation (left) and 60 degree orientation (right). Note, the WEC outline appears to “rotate” when comparing the left and right images since the sonar scan is still oriented along the flume axis, and not along the WEC axis. Note 2, the wave train proceeds from left to right in the bathymetry scans.

Influence of Test Apparatus

Inclusion of the lift frame was not a large factor in the present experiments. In particular, wave 3 was investigated with and without the lift frame, using the standard caisson. The extent of scour is nominally identical, with only small subtle differences in local scour/accretion. (see figure 43).

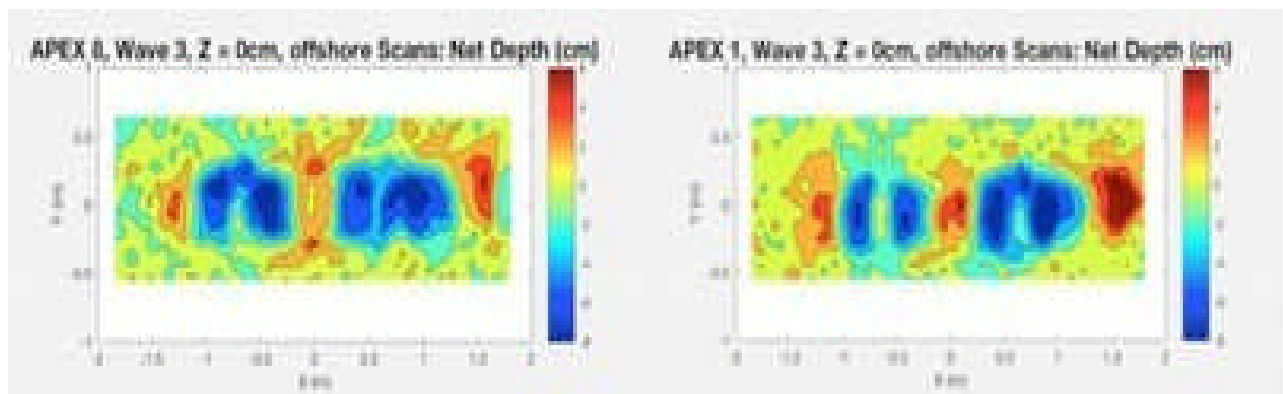


Figure 43. Net bathymetry comparison of the standard caisson WEC after wave 3 with the lift frame (left), and without the lift frame (right).

Suction pile WEC deployment was successful in pulling the piles into the sand, and embedding the WEC. Further, the standard caisson WEC was able to be situated at heights between 40cm and 5cm above the sandy bottom using a combination of suction pile height and amount of suction embedment. Wave 1 was run over the suction piled WEC at heights of 5cm and 20cm elevation, and in both cases, the WEC was stable as viewed by live, close-up video inspection during wave operation. Further, the WEC was very difficult to remove from the seabed after suction embedment.

Next-Generation Design

Combining the improvements identified during the course of this project yields a potential next-generation design.

Design attributes of next-generation design:

1. 25%-50% reduction in caisson side walls
2. Lower plane of device elevated off bottom by 0.5m-0.75m or more
3. Anchoring achieved by suction piles or similar rigid mounting to sea floor
4. Primary structural material: Fiber-Reinforced Polymer (FRP).

An example of a potential next-generation design is shown in Figure 44.

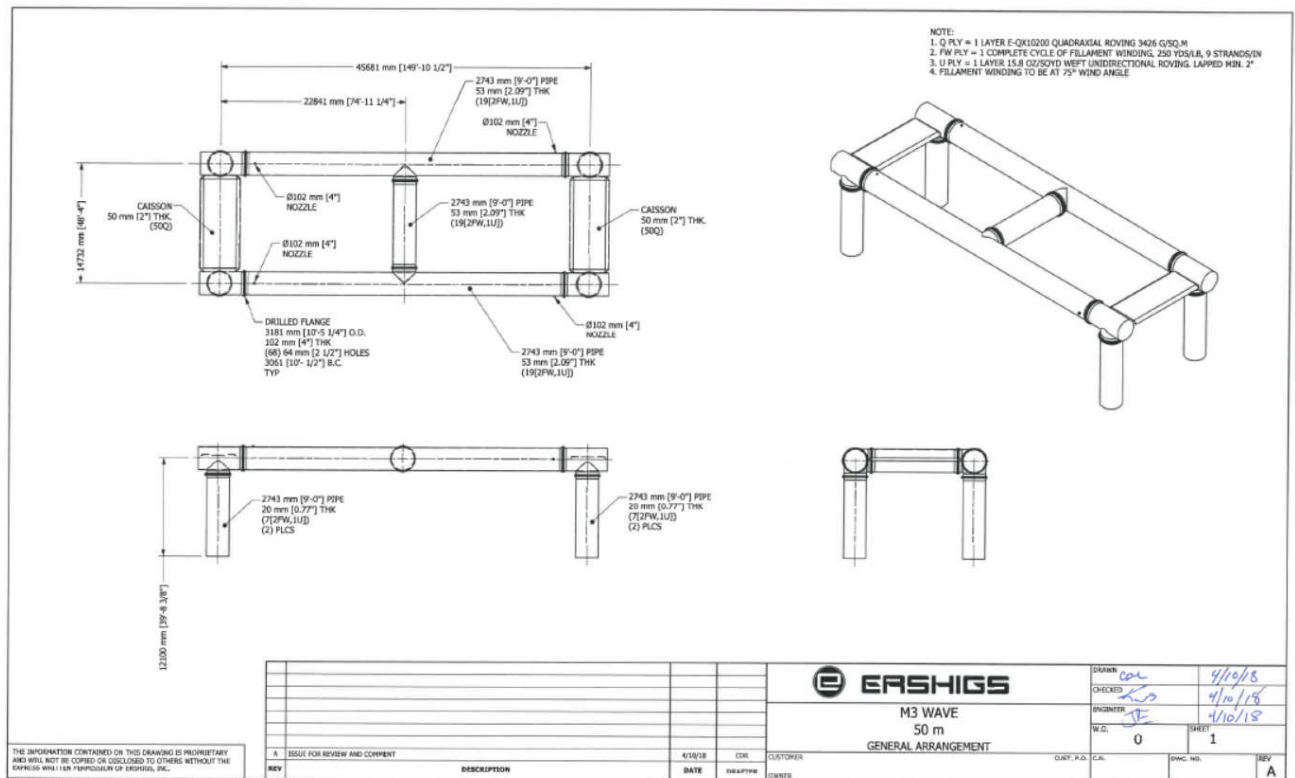


Figure 44: Design concept for an all-FRP APEX design.

Appendix B contains preliminary FEA analysis confirming that FRP is a suitable structural material.

Analysis / Conclusions

This project achieved all project objectives. Multiple analytical methods and techniques were developed that can be applied towards any rigid body mounted on or near the sediment bed. These

tools were validated with empirical testing. During the course of this project, design changes were identified that will mitigate the impact of sediment transport on device survivability, improving AEP. These changes include modifications to anchoring strategy which will enable use of lightweight materials, reducing CAPEX and deployment cost.

The generally accepted important factors regarding scour of an object at or near the seabed were empirically explored, and confirmed to have the expected impacts. The general scour results from previous 1:25 testing were confirmed at 1:5 in the large wave flume. These results provided a rich data set for validating to numerical scour model predictions.

While the suction pile instantiation was not unique within this testing in terms of testing the effect of elevation on scour, it was instructive regarding possible future deployments. With some seabed compositions, suction piles can be used to secure a WEC to the seabed, and can effectively be used to level the WEC. We found that we could lower the WEC, and level the WEC to any desired configuration between 5cm and 20cm of elevation. Of course, with longer piles, greater elevation can also be achieved.

Key design parameters were identified for mitigating sediment transport and improving survivability:

- Minimizing surfaces and geometries that can cause hydrodynamic accelerations (“skeleton” or “minimalist” caisson),
- Elevating the primary geometry off the ocean floor by 0.25m-0.7m (at full scale)
- Using suction piles or similar embedment anchoring to achieve desired elevation while decoupling the need to add anchor mass to the device.

Metric	Baseline Value	Target Value	Projected Actual	Assumptions
CAPEX (\$/kW) at array scale	\$8,000	\$6,000	\$4,200	FRP structure 30% savings Towing cost 50% savings Tending vessel 2x more expensive (suction piles)
AEP (Mwh/year per discrete device)	133	300	292	Availability improves to 55% vs 25% baseline (scour-induced shutdown)
LCOE (\$/kW-h) at array scale	\$0.80-\$1.10	\$0.20-\$0.50	\$0.202	Primarily driven by CAPEX reduction and AEP improvement
Levelized O&M at array scale (\$M/year; 1,000 discrete devices)	3.2	2	2.3	50% savings in technicians and tending vessels due to less sediment-related interventions.

References

- [1] Aurélien Babarit, Fabian Wendt, Y-H Yu, and Jochem Weber. Investigation on the energy absorption performance of a fixed-bottom pressure-differential wave energy converter. *Applied Ocean Research*, 65:90–101, 2017.
- [2] Nils RB Olsen and Morten C Melaaen. Three-dimensional calculation of scour around cylinders. *Journal of Hydraulic Engineering*, 119(9):1048–1054, 1993.
- [3] B Mutlu Sumer and Jørgen Fredsøe. *The mechanics of scour in the marine environment*. World Scientific, Singapore, 2002.
- [4] WAMIT. *WAMIT User Manual*. Chestnut Hill, MA, 7 edition, 2012.
- [5] Wen Xiong, CS Cai, Bo Kong, and Xuan Kong. Cfd simulations and analyses for bridge scour development using a dynamic-mesh updating technique. *Journal of Computing in Civil Engineering*, 30(1):4010-4121, 2014.

Publications associated with this project:

Presented at Coastlab2018 in Santander, Spain, May, 2018.

PHYSICAL MODEL TESTING OF THE SCOUR INDUCED BY APEX, A SUBMERGED PRESSURE DIFFERENTIAL WAVE ENERGY CONVERTER

PEDRO LOMONACO¹, BRET BOSMA¹, MIKE DELOS-REYES², ALICE GILLESPIE², TIM MADDUX¹, MIKE MORROW², TUBA ÖZKAN-HALLER³

¹Hinsdale Wave Research Laboratory, Oregon State University, United States, Pedro.Lomonaco@oregonstate.edu

²M3 Wave LLC, United States, mike@m3wave.com

³College of Earth, Ocean, and Atmospheric Sciences, Oregon State University, United States, Tuba.Ozkan-Haller@oregonstate.edu

1 INTRODUCTION

M3Wave, LLC have developed a submerged, stationary Wave Energy Converter (WEC) that transforms wave pressure into electricity. Unlike many conventional ocean power devices, this WEC resides entirely under the surface of the ocean. Fundamentally, the device consists of two airbags interconnected by a pipeline containing a reversible wind turbine. The airbags are self-contained by a single structure which upholds the device stationary and keep a constant separation of the airbags. The pressure differential observed under waves forces the air to flow from one of the airbags to the other, and through the air turbine, driving an electrical generator and producing energy.

In 2014, M3Wave deployed this submerged pressure differential Wave Energy Converter in Camp Rilea, (Sunset Beach) Oregon, at roughly 15 m depth and over sandy bottom. At the end of the testing period, the divers reported scour around and underneath the device. Moreover, after analyzing the data, it turns out that the device stopped producing energy and there was no evidence of a malfunctioning system. It has been proposed that the scour introduced some tilt in the device, where an angle in excess of 7° may prevent the flow of air and, thus, energy production.

The assessment of scouring induced by the device under different wave conditions and incident angles, as well as the implementation of mitigation measures, were deemed necessary to ensure the reliability of the device, as well as to assess potential environmental effects. Physical modeling remains the most efficient and reliable way to accomplish the aforementioned objectives.

2 LARGE-SCALE PHYSICAL MODEL TESTING

Mobile-bed physical model tests of the scour potential of a 1:5 scale model of a submerged pressure differential device have been tested in the Large Wave Flume (LWF) at the Hinsdale Wave Research Laboratory, Oregon State University. The flume measures 104 m long by 4.6 m deep by 3.6 m wide, and has a dry-back piston-type wave maker with a 4 m stroke capable of generating large tsunami, periodic or random waves for the purposes of scaled model tests.

The piece-wise concrete bathymetry was deployed along the flume to create a horizontal platform elevated 55 cm from the original flume bottom, and followed by a 1:12 sloping beach for wave dissipation (Figure 1). At the horizontal platform, a 11 m long sand pit was installed, filled with approximately 30 m³ of sand retrieved from the Oregon coast.

The flume was filled to its maximum depth of 2.7 m, yielding a water depth of close to 2.2 m at the test section. The 1:5 scale WEC model was then installed and tested under a range of wave conditions and mitigation measures (i.e. modifications in the airbag container permeability, orientation of the device, and elevation of the device).

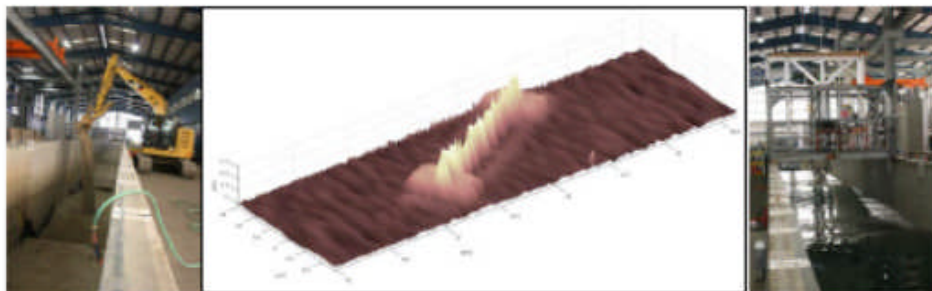


Figure 1. a) Construction of the sand pit and bathymetry, b) Measured bottom features at the test section, including the WEC installed at an oblique angle, and c) Testing of the WEC under regular waves.

The measured parameters during the testing included resistive-type wave gauges to capture the wave evolution before and after the location of the WEC, 6 Vectrino-II ADVs probes to describe the velocity profile before and after the WEC device, 32 ultrasonic ranging probes to measure the sea-bed evolution, and 2 on-board Vectrino-II ADVs to measure the WEC wake properties and scouring potential.

The final paper will describe the test layout, measurement procedures, and results on the scour induced by the near-bed pressure differential WEC, as well as the impact of the mitigation measures to prevent scouring.

SANDIA REPORT

SAND2017-XX
Unlimited Release
Printed XX

An approach for shear-stress based scour prediction

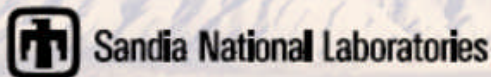
Ryan G. Coe, Chris Chartrand, Jesse Roberts, Sterling Olson, and Craig Jones

Prepared by
Sandia National Laboratories
Albuquerque, New Mexico 87185 and Livermore, California 94550

Sandia National Laboratories is a multi-mission laboratory managed and operated by National Technology and Engineering Solutions of Sandia, LLC, a wholly owned subsidiary of Honeywell International, Inc., for the U.S. Department of Energy's National Nuclear Security Administration under contract DE-NA0003525.

Approved for public release; further dissemination unlimited.

DRAFT



Additional papers and derivative works may be published in the months to come.

Appendix A

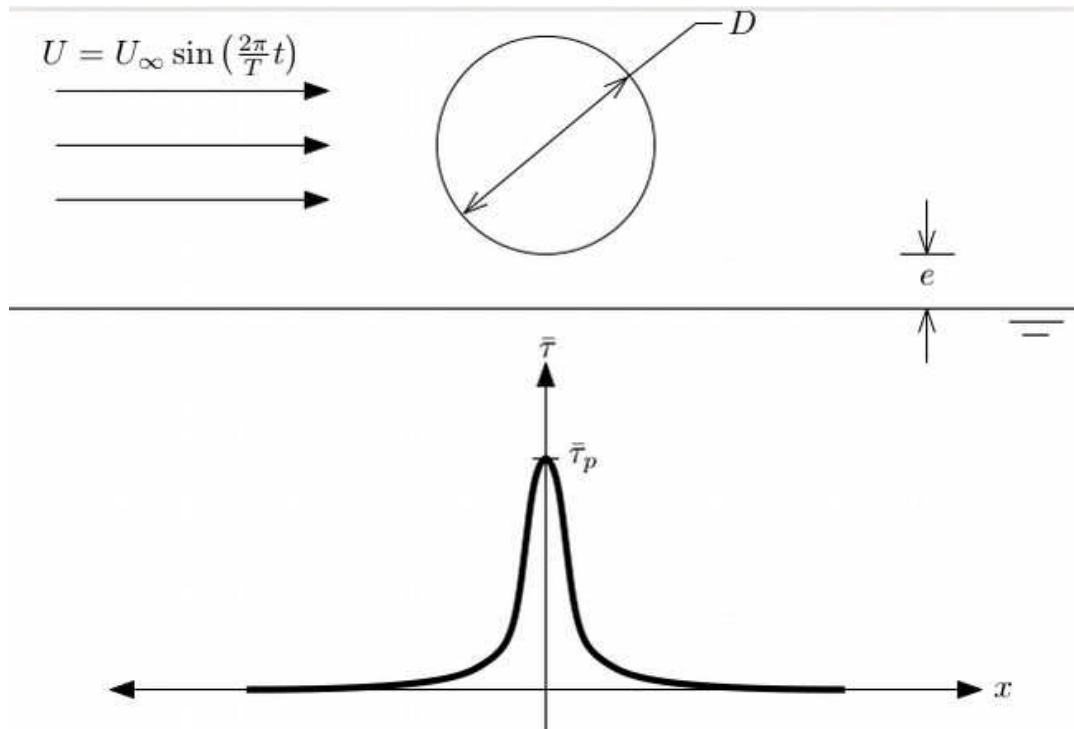


Figure A.1: Diagram of 2D flow over pipe simulation with shear stress map.

A

Investigating 2D pipe scour

CFD simulations were conducted in OpenFOAM using the configuration depicted in Figure A.1 for a variety of KC numbers. The unsteady RANS simulations were run with using the *pimpleFoam* solver with an adjustable time step that enforced the condition $CFL < 0.25$ throughout the entire domain. The computational grid was generated in Pointwise with a wall spacing set to $\Delta x_{\text{wall}} = 0.005D$, expanding out to a far field discretization of $\Delta x_{\text{far}} \approx D$. Illustrations of the grid used for one of the $D = 2$ simulations are shown in Figures A.2 and A.3. Example results from a simulation are shown in Figure A.4.

Here, oscillating flow, with a velocity of $U = U_{\infty} \sin\left(\frac{2\pi}{T}t\right)$ is simulated over a cylinder with diameter D . As some 2D pipe scour (that which is due to jetting beneath the pipe) is initiated by a pressure differential, not shear stress, the simulation is configured with a cylinder offset from the sea floor by some small distance e , which varied between $0.025D$ and $0.2D$ in these simulations. The simulation configuration depicted in Figure A.1 was evaluated by finding the period-averaged shear stress, $\bar{\tau}$, along the stream-wise dimension, x (see lower half of Figure A.1). From the averaged shear stress, the peak value of the distribution, $\bar{\tau}_p$, is extracted.

A series of simulations were run with varying values of KC. This was accomplished by varying the velocity, U_{∞} , pipe diameter, D , and period oscillation, T . Table A.1 shows the simulations

performed for this study In addition to the simulation parameters, peak average shear, $\bar{\tau}_p$, KC number, scour depth, S, scour width, W, and a scour parameter to be subsequently discussed, ζ , are presented. As expected, $\bar{\tau}_p$, was observed to be proportional to the velocity squared.

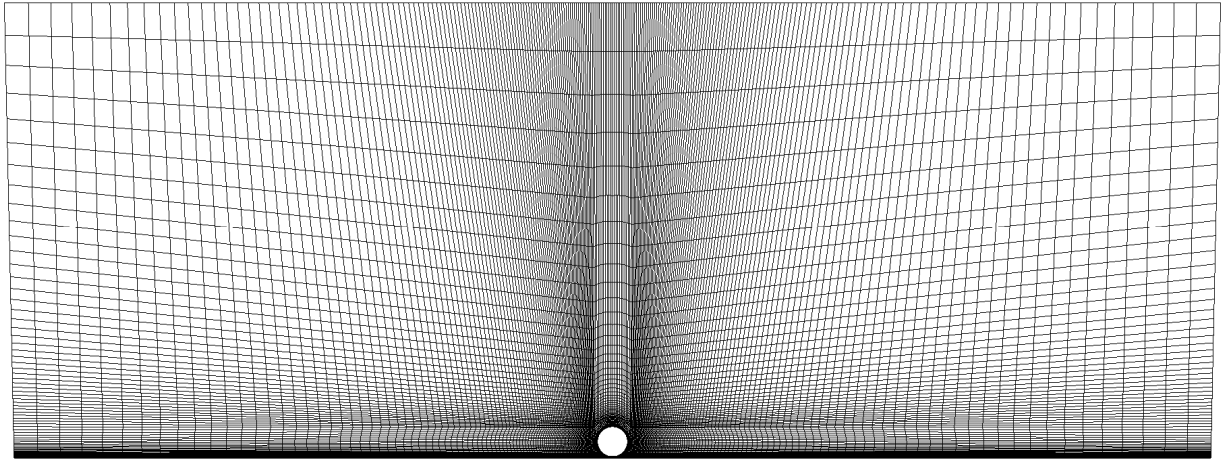


Figure A.2: Computational grid used for numerical analysis.

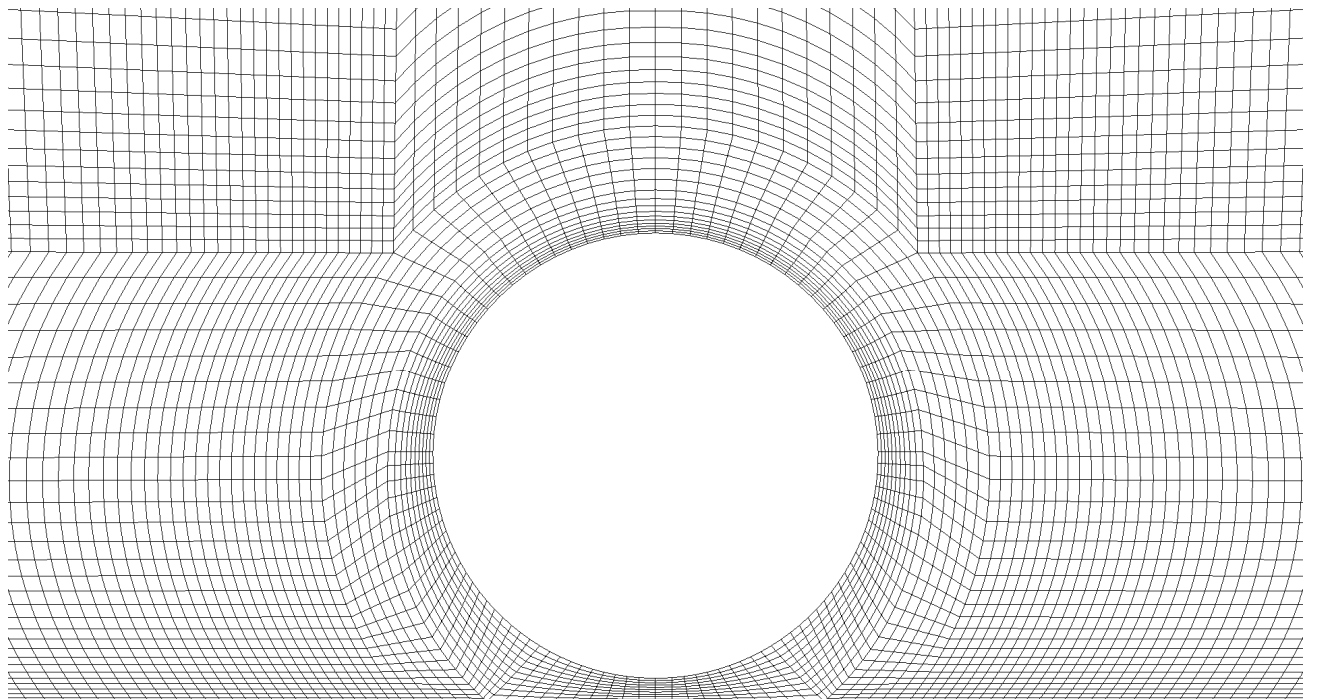


Figure A.3: Close up zoom of the numerical grid.

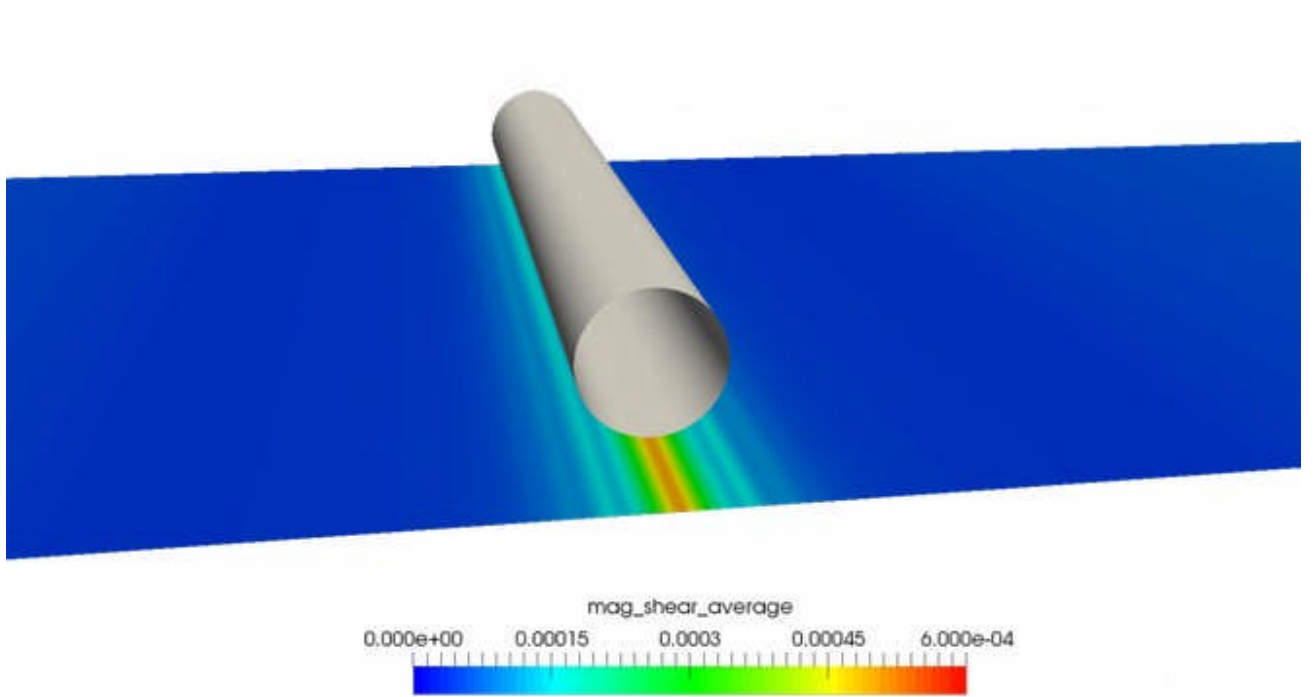


Figure A.4: OpenFOAM results for simulated wave over 2D pipe with $U = 0.4$ m/s and $T = 16$ s.

$$\bar{\tau}_p \propto U_\infty^2 \quad (8)$$

Knowing the trend described by (1), we considered a new quantity based on $\bar{\tau}_p$.

$$\zeta = \frac{\sqrt{\bar{\tau}_p T D}}{U \rho} \quad (9)$$

The quantity ζ has dimensions of length.

$$\left(\frac{[mass]}{[length][time]^2} \frac{[time]}{1} \frac{[length]}{1} \frac{[time]}{[length]} \frac{[length]^3}{[mass]} \right)^{\frac{1}{2}} = [length] \quad (10)$$

Testing this new quantity, we find that it shows a strong linear correlation with scour. This trend is shown in Figure A.5. Figure A.5 shows data for offsets of $e = 0.05$, and 0.1 m, shown in red and blue respectively. A black dashed line (with $r^2 = 0.988$) in Figure A.5 shows the overall trend. This is given by

Offset, e [m]	Diam., D [m]	Vel., U [m/s]	Per., T [s]	Shear, τ_p [Pa]	KC []	S [m]	W [m]	ζ [m]
0.05	1	0.4	16	6.27×10^{-4}	6.4	0.25	1.17	0.16
0.05	1	0.8	8	2.12×10^{-3}	6.4	0.25	1.17	0.15
0.05	1	1	6.4	3.19×10^{-3}	6.4	0.25	1.17	0.14
0.05	1	1.2	20	5.5×10^{-3}	24	0.49	2.76	0.3
0.05	1	2	16	1.44×10^{-2}	32	0.57	3.33	0.34
0.05	1	0.5	16	9.7×10^{-4}	8	0.28	1.35	0.18
0.05	1	1	20	3.88×10^{-3}	20	0.45	2.45	0.28
0.05	1	2	16	1.44×10^{-2}	32	0.57	3.33	0.34
0.1	1	0.4	16	4.64×10^{-4}	6.4	0.25	1.17	0.14
0.1	1	0.8	8	1.37×10^{-3}	6.4	0.25	1.17	0.12
0.1	1	1	6.4	2.05×10^{-3}	6.4	0.25	1.17	0.11
0.1	1	1.2	20	5.18×10^{-3}	24	0.49	2.76	0.29
0.1	2	2.4	20	1.85×10^{-2}	24	0.98	5.52	0.56
0.1	1	2	16	1.36×10^{-2}	32	0.57	3.33	0.33
0.1	1	0.5	16	7.94×10^{-4}	8	0.28	1.35	0.16
0.1	1	1	20	3.62×10^{-3}	20	0.45	2.45	0.27
0.1	1	2	16	1.36×10^{-2}	32	0.57	3.33	0.33
0.1	2	0.5	16	7.32×10^{-4}	4	0.4	1.72	0.22
0.1	2	1	20	3.41×10^{-3}	10	0.63	3.13	0.37
0.1	2	1.6	20	8.49×10^{-3}	16	0.8	4.24	0.46
0.1	1	0.1	10	2.91×10^{-5}	1	0.1	0.35	0.05

Table A.1: 2D flow over pipe cases considered for this study.

$$(11) \quad S = 1.6706 \zeta + 0.0141$$

The high degree of accuracy in this trend essentially affirms that $\tau \propto U^2$. However, the coefficients in (11) are specific to flow under a pipe-like body.

Note that ζ is defined partially by some characteristic dimension, D. This parameter, while somewhat inconvenient, is believed to incorporate the same connection to turbulence scale, which is known to be an important factor for scour in waves [3]. In order to apply (9) to some arbitrary geometry, a single characteristic length, D, must be defined.

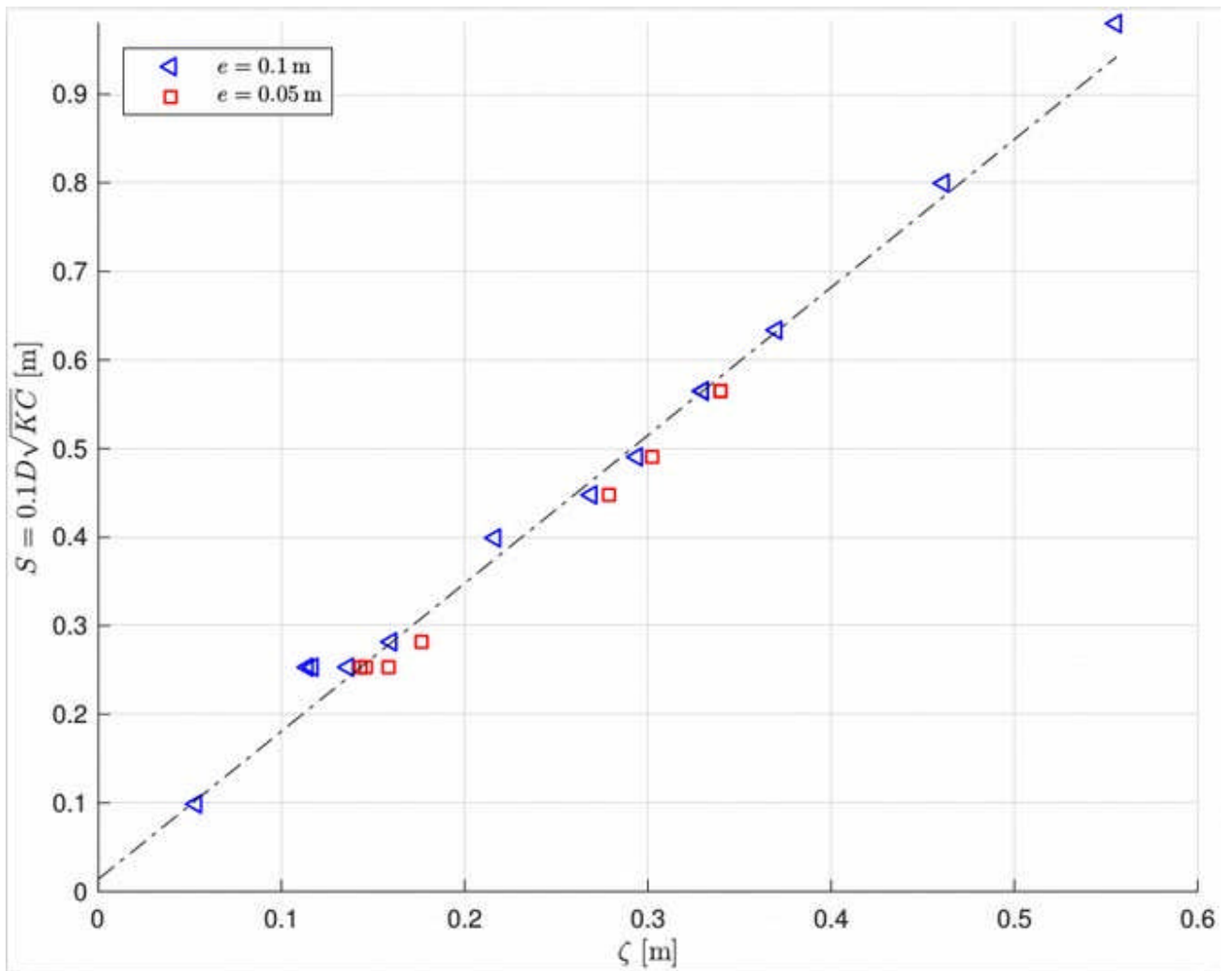


Figure A.5: Correlation of peak shear stress quantity, $\zeta = \sqrt{(\bar{\tau}_p T D / (U\rho))}$, and scour, $S = 0.1D\sqrt{KC}$. Linear trend of $S = 1.6706\zeta + 0.0141$ has $r^2 = 0.988$.

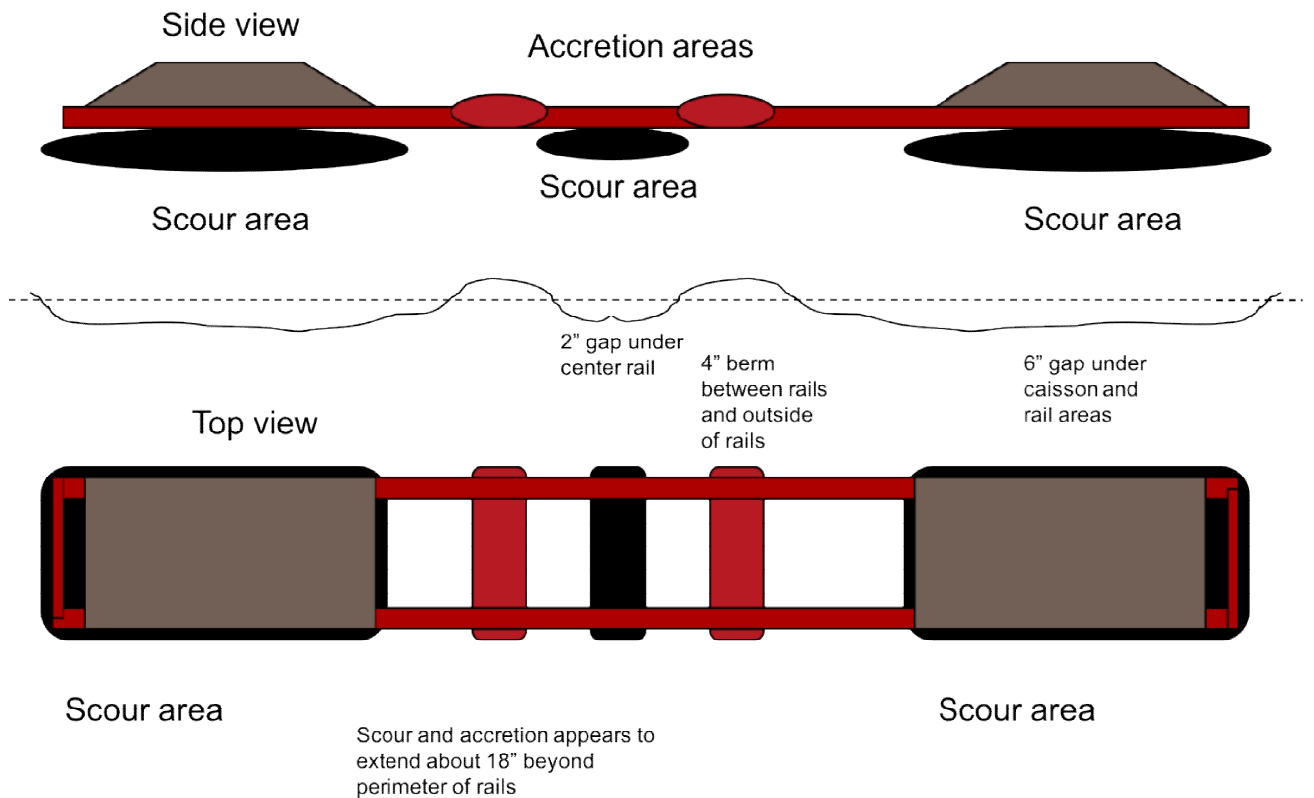


Figure B.6: Qualitative scour under M3 Apex device based on at-sea deployment.

B Apex CFD scenes

In order to assess the ability of the trend developed in Section 3, here we consider the M3 Apex device. An at-sea deployment was conducted with the Apex device. During this deployment, the device was subjected to a wide range of wave conditions. In addition to variation in spectral content, the wave heading also varied during this deployment. Additionally, the sediment on which the device was situated for this deployment was non-homogeneous. Qualitative observations of this device showed roughly 6 in of scour underneath the frame of the device (see Figure B.6).

The procedure for this assessment utilized the following steps:

1. Perform CFD simulations with M3 Apex device (conditions shown in Table B.2)
2. Knowing that the observed scour was 6 in (~ 15 cm), reformulate (11) as

$$D = \frac{U\rho}{\tau T} \left(\frac{S - 0.0141}{1.6706} \right)^2$$

(12)

3. Find the characteristic dimension, D , using (12) for each CFD simulation

4. Compare the calculated characteristic dimension with the actual dimensions of the M3 device.

ID	Offset, e [m]	Velocity, U [m/s]	Period, T [s]	τ_m [Pa]	$\bar{\tau}_p$ [Pa]	$D(\tau_m)$ [m]	$D(\bar{\tau}_p)$ [m]
1	0.01 (A)	0.16	8.3	8.70E-04	4.07E-04	0.152	0.324
2	0.01 (B)	0.4	16	2.18E-03	9.85E-04	0.0784	0.195
3	0.05	0.4	16	2.69E-03	1.17E-03	0.0638	0.146
4	0.1	0.4	16	2.53E-03	1.02E-03	0.0678	0.168

Table B.2: Shear-based prediction of scour for M3 Apex.

The results of this study are summarized in Table B.2. Note that in addition to the peak of the period-averaged shear stress ($\bar{\tau}_p$), Table B.2 also presents results for the peak of the maximum shear stress (τ_m). Scalar images of $\bar{\tau}_p$ and τ_m are shown in Appendix B. From Table B.2, we can see that for the majority for the cases considered, the characteristic dimension, when using $\bar{\tau}_p$ is close to the $D = 6$ in observed in the at-sea deployment.

This Section contains a number of rendered scenes from CFD simulations of the M3 Apex device. In each figure, the results are shown (clockwise from the upper left) for simulation 1, 2, 3, and 4 in Table B.2.

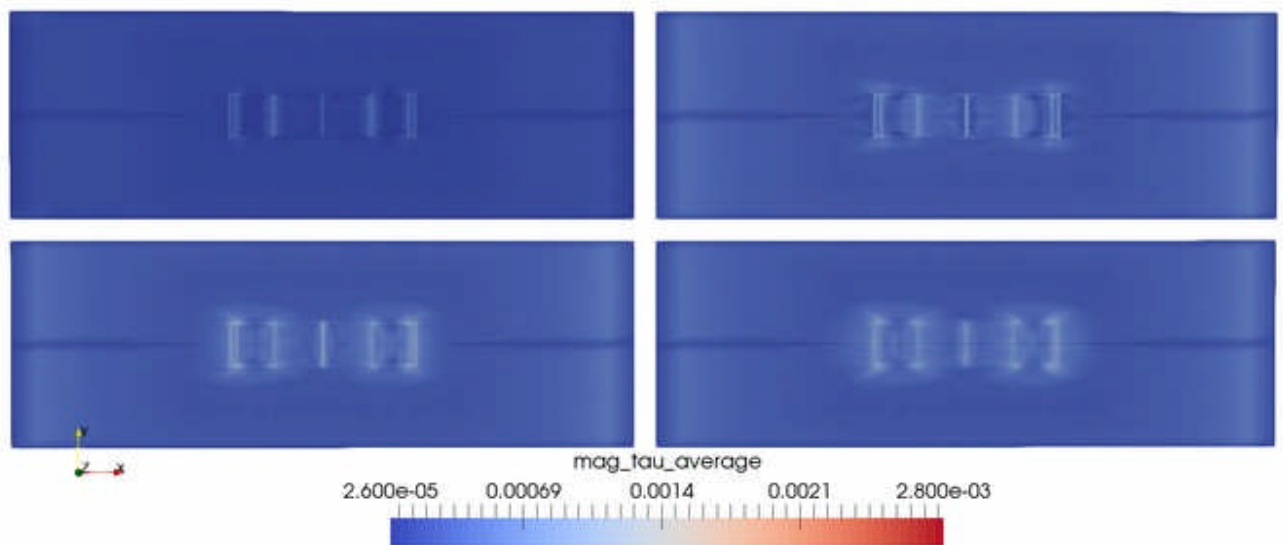


Figure B.7: Comparison of $\bar{\tau}_p$ for M3 Apex simulations listed in Table B.2. Simulation results are shown (clockwise from the upper left) for simulation 1, 2, 3, and 4 in Table B.2.

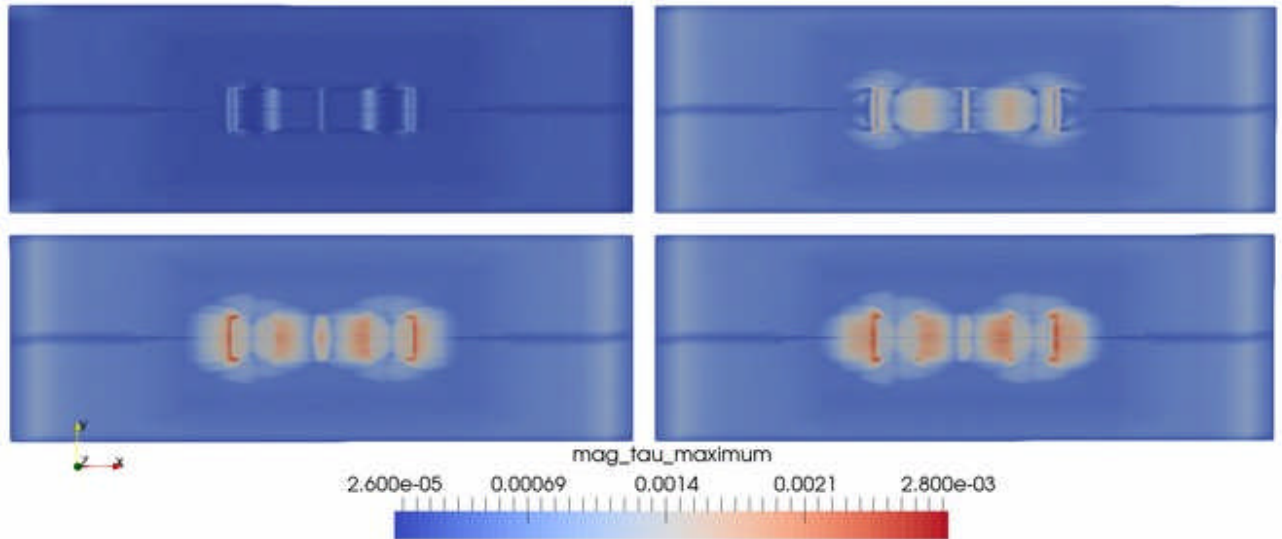


Figure B.8: Comparison of τ_m for M3 Apex simulations. Simulation results are shown (clockwise from the upper left) for simulation 1, 2, 3, and 4 in Table B.2.

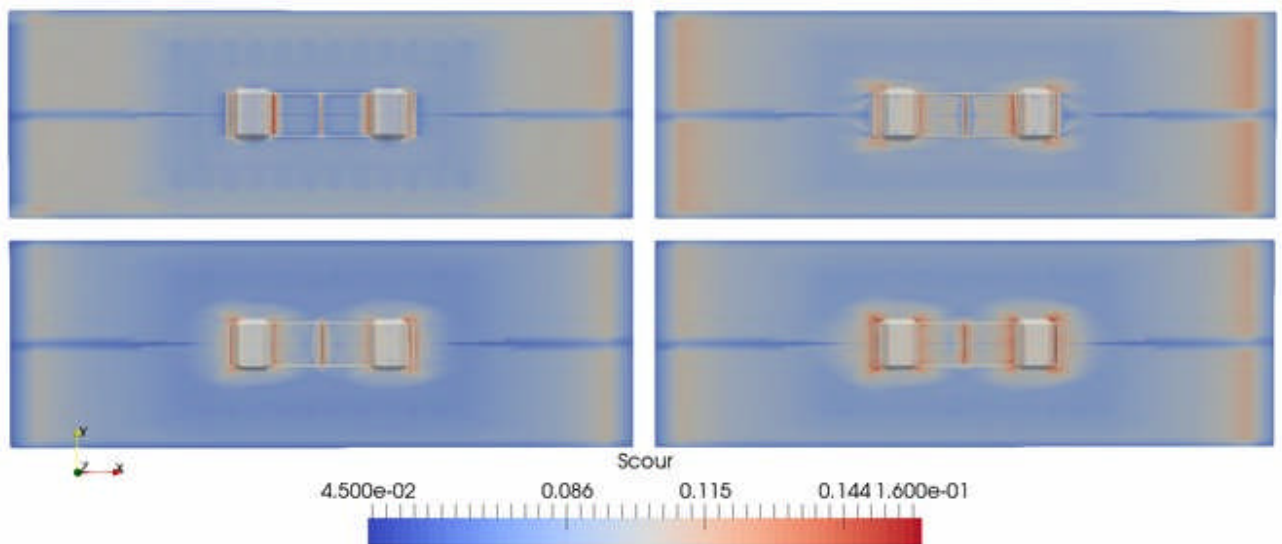


Figure B.9: Scour based on $\bar{\tau}_p$ for M3 Apex simulations. Simulation results are shown (clockwise from the upper left) for simulation 1, 2, 3, and 4 in Table B.2.

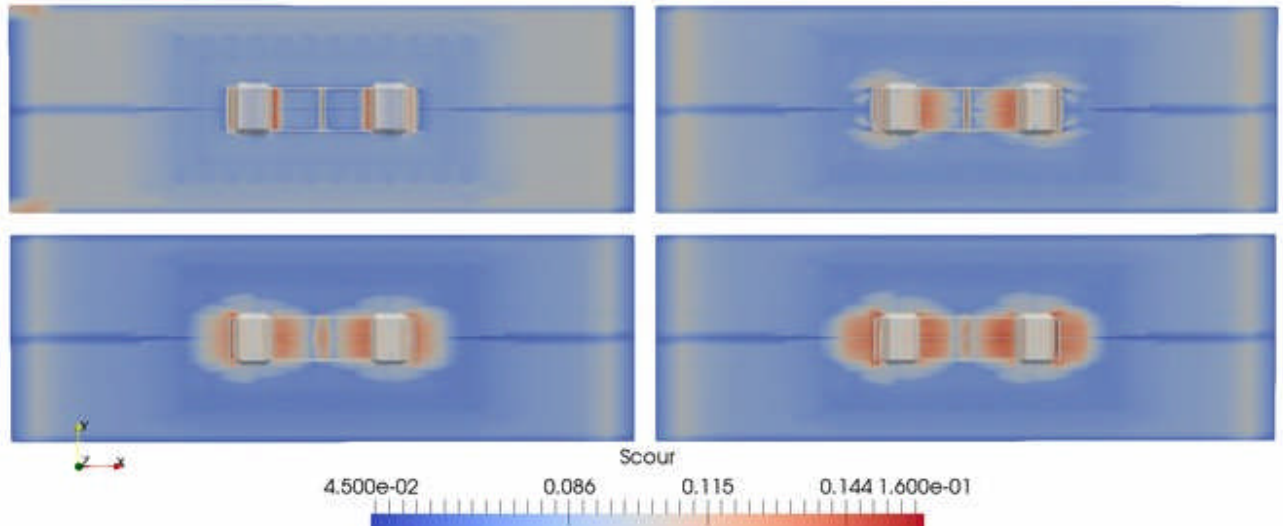


Figure B.10: Scour based on τ_m for M3 Apex simulations. Simulation results are shown (clockwise from the upper left) for simulation 1, 2, 3, and 4 in Table B.2.

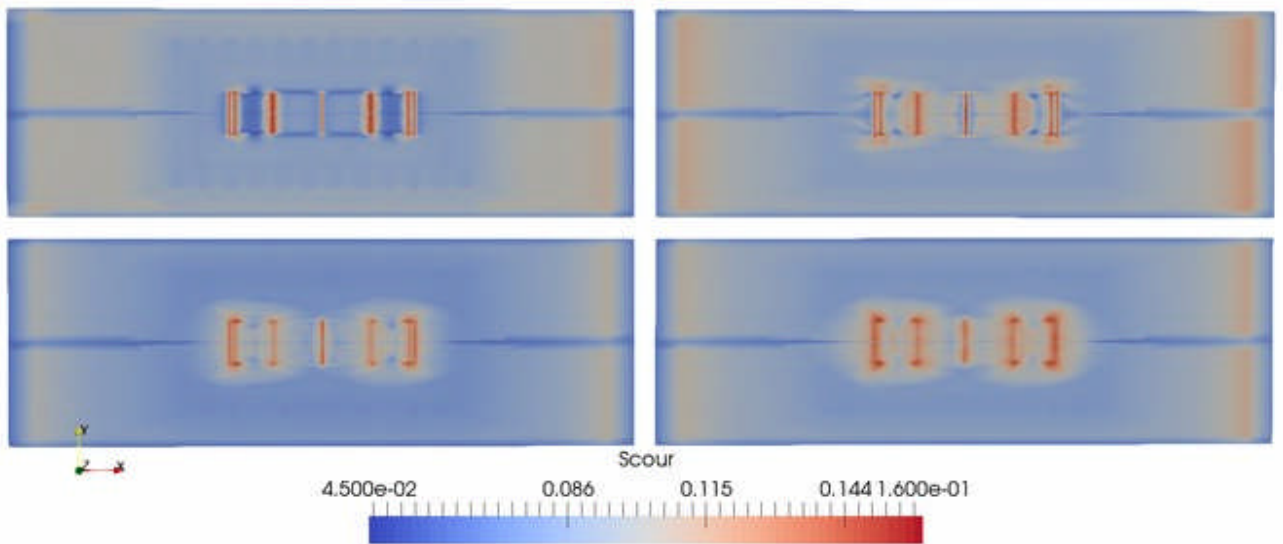


Figure B.11: Scour based on τ_p for M3 Apex simulations (no device shown). Simulation results are shown (clockwise from the upper left) for simulation 1, 2, 3, and 4 in Table B.2.

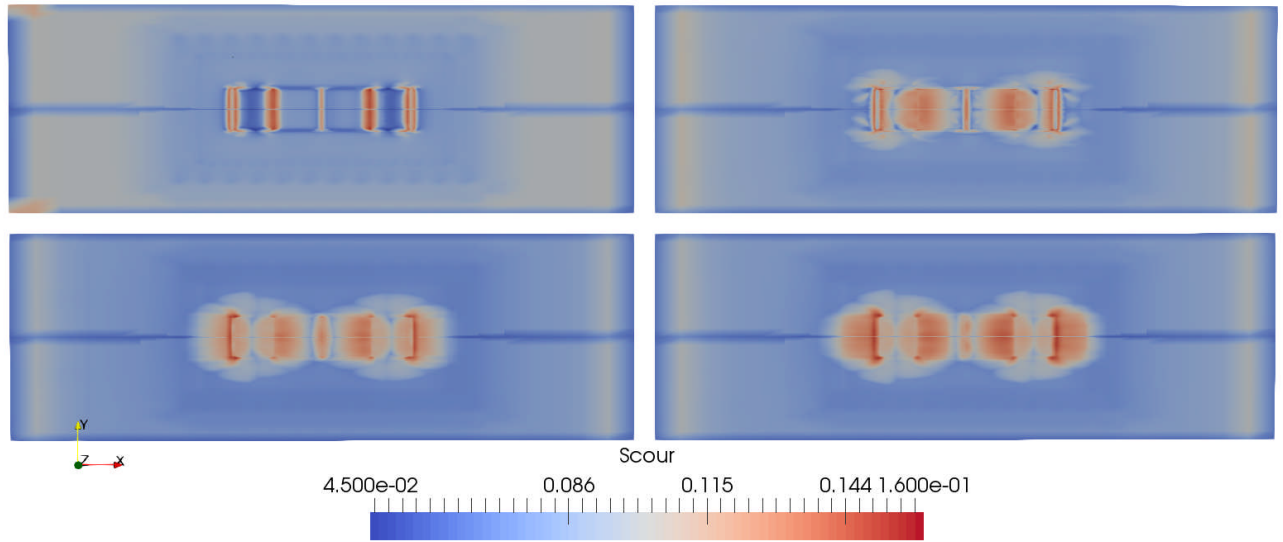


Figure B.12: Scour based on τ_m for M3 Apex simulations (no device shown). Simulation results are shown (clockwise from the upper left) for simulation 1, 2, 3, and 4 in Table B.2.

Appendix B: FEA of Composite version of APEX



ERSHIGS

M3 Wave

10m & 50m APEX

FEA Report

By: J. Eastin, PE

**Ershigs Control Number:
Ershigs Work Order Number:**

**Revision A
May 30, 2018**

M3 WAVE
10m & 50m APEX
FEA REPORT

Rev	Date	By:	Description:
A	05-30-18	JE	Design Concept

Revision Log:

M3 WAVE
10m & 50m APEX
FEA REPORT

1 <u>SUMMARY</u>	3
2 <u>DESIGN DATA</u>	3
2.1 MATERIAL PROPERTIES	3
2.2 ACCEPTANCE CRITERIA	4
2.3 LOADS.....	4
3 <u>RESULTS</u>	5
3.1 10m APEX	5
3.2 50m APEX	7
4 <u>CONCLUSION</u>	9

SUMMARY

ANSYS Workbench 18.0 was used to perform a Finite Element Analysis (FEA) in order to verify the feasibility of using FRP in the design of the structural components for the 10m and 50m APEX. This is currently for design conceptualization only and focusses on two (2) components (caisson and frame) for both the 10m and 50m APEX systems. Detailed component connections, assembly, component internals and lifting/submerging plans have not been addressed, as this would take place during the detailed design/engineering phase.

2 DESIGN DATA

2.1 MATERIAL PROPERTIES

For purposes of the initial concept it was assumed that the Caissons would be an infused laminate (VectorPly E-QX10200 was used for this analysis) and that the frame components would be Filament Wound (FW) using 55degree winding with Uni-directional layers for additional axial support. Note that these are just general assumptions used for the conceptual analysis and that other laminate processes/orientations may prove to be more suitable under detailed design analysis or due to fabrication/assembly requirements.

The properties for the materials applied to the components in the FEA model are shown below.

Infused Laminate (Caisson)
 Density 8.e-002 lbm in⁻³

Temperature F	Young's Modulus X direction	Young's Modulus Y direction	Young's Modulus Z direction	Poisson 's Ratio XY	Poisson 's Ratio YZ	Poisson 's Ratio XZ	Shear Modulus XY psi	Shear Modulus YZ psi	Shear Modulus XZ psi
	3.72e~00	2.33e~00	1	0.31	0.27	0.26	8.34e~00	6.e~00	5.45e~00

The X and Y-axis property orientations (above) were applied for long and short-axis directions of the top plate of the Caisson, respectively. Z-axis is through the thickness of the plate.

FW Laminate (Frame)
 Density 6.2e-002 lbm in⁻³

Temperature F	Young's Modulus X direction	Young's Modulus Y direction	Young's Modulus Z direction	Poisson 's Ratio XY	Poisson 's Ratio YZ	Poisson 's Ratio XZ	Shear Modulus XY psi	Shear Modulus YZ psi	Shear Modulus XZ psi
	1.7e~00	3.8e~00	1.2e~00	0.11	0.32	0.31	4.11e~00	3.74e~00	4.35e~00

M3 WAVE

10m & 50m APEX

FEA REPORT

or the FW frame sections the X and Y-axis properties correspond to the axial and hoop direction of the laminate, respectively. Z-axis is again through the thickness.

2.2 ACCEPTANCE CRITERIA

The maximum allowable stress for the infused laminate used for the Caissons is 6000psi. This is based on a 10:1 design factor on the ultimate strength of this particular infused laminate (60ksi).

For the FW frame the allowable stress is based on a 0.00 1 in/in strain limit based on the axial/hoop tensile fiber direction. This results in maximum allowable stresses of 1700psi and 3800psi in the axial and hoop directions, respectively.

2.3 LOADS

For the Caisson analysis, a buoyancy load from the air bag was applied acting upwards on the inside surface of the top panel. The load was assumed to be evenly distributed across the entire surface. The loads for the 10m and 50m models were 3.5kips and 150kips, respectively. The image below illustrates the load as applied to the 50m APEX.

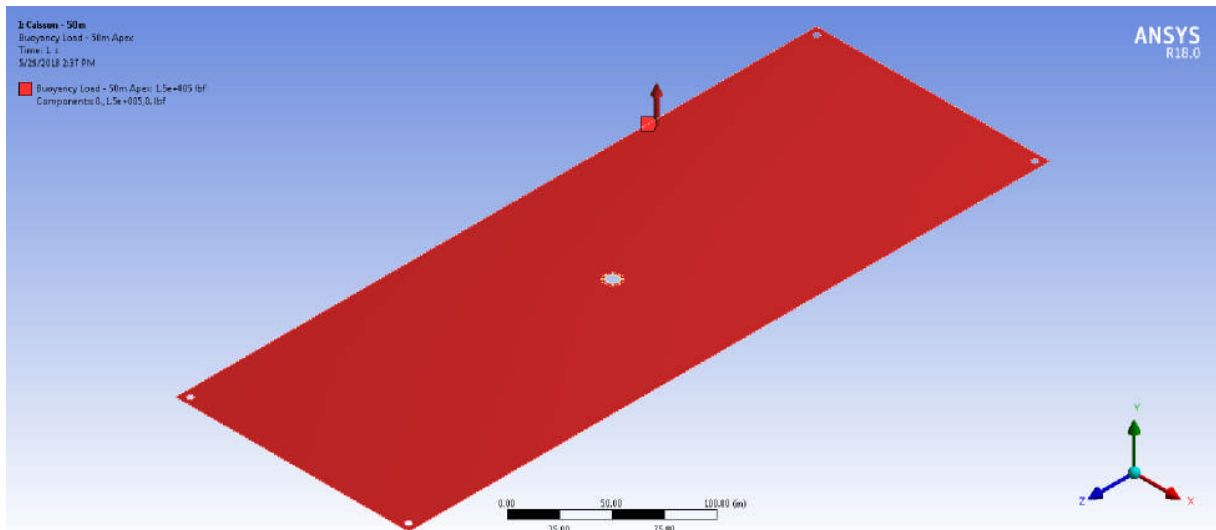


Figure 1: Caisson Load (50m APEX)

For purposes of this analysis the panel was fixed translationally at all edges, but allowed to deform rotationally. The flange connection at the center of the panel was assumed to be a rigid connection, and was not allowed to deform rotationally. Not that for this analysis only the top panel was evaluated and all other panels Caisson panels are just assumed to be the same thickness for this stage of the conceptual design. Also note that no internal features or stiffeners were considered at this stage.

The long beam of the frame was also analyzed for both the 10m and 50m. The end of each beam was loaded with the approximate weight of one (1) Pile Anchor (also assumed to be FRP) and half of the weight of the Caisson and air bag. This resulted in loads of 1.4kips and 22kips at each end of the 10m and 50m frames, respectively (illustrated below).

M3 WAVE
10m & 50m APEX
FEA REPORT

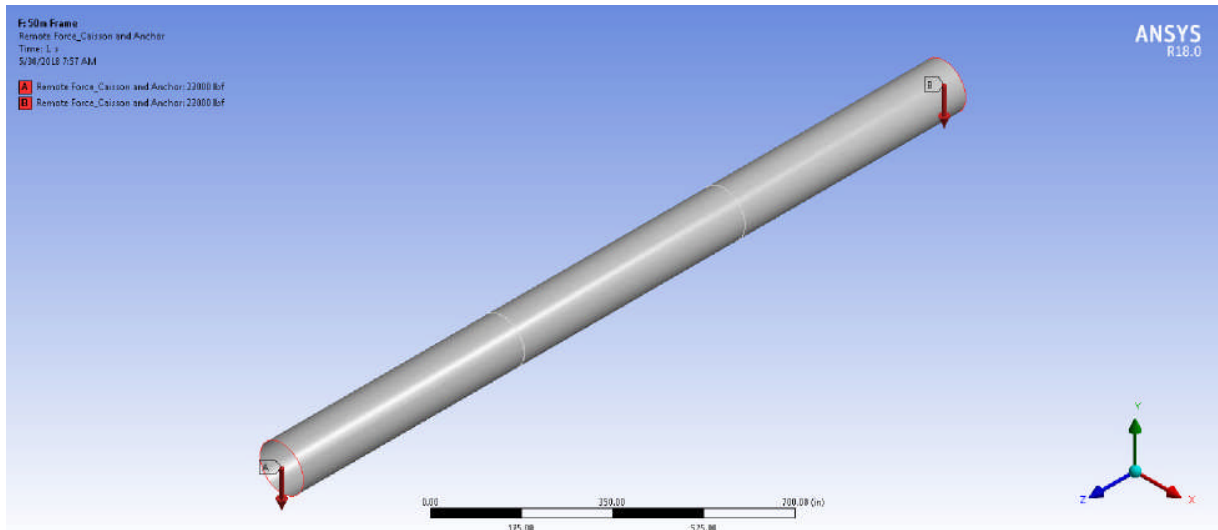


Figure 2: Frame Load (50m APEX)

For this analysis it was assumed that frames would be supported at two (2) locations equally spaced along the length of the beam (shown in yellow, below) for lifting. Note that detailed lifting lugs have not been modeled/evaluated at this stage. Also, the weights at this stage do not include any potential joint/flange/connection weights.

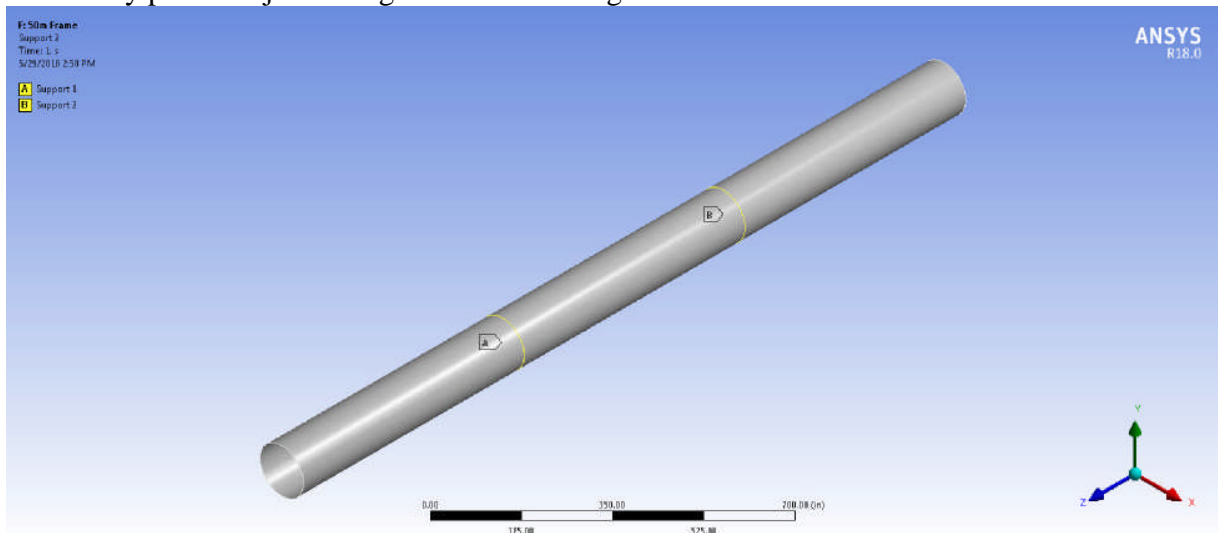


Figure 3: Lifting Locations (50m APEX)

3 RESULTS

3.1 10m APEX

The following plots depict the maximum stresses in the Axial and Transverse directions (X and Y-axis material orientations, respectively) of the infused panel for the 10m APEX. Note that the deflection has been magnified significantly in order to illustrate the load direction/deflection. The panel is modeled at 0.58” thick.

**M3 WAVE
10m & 50m APEX
FEA REPORT**

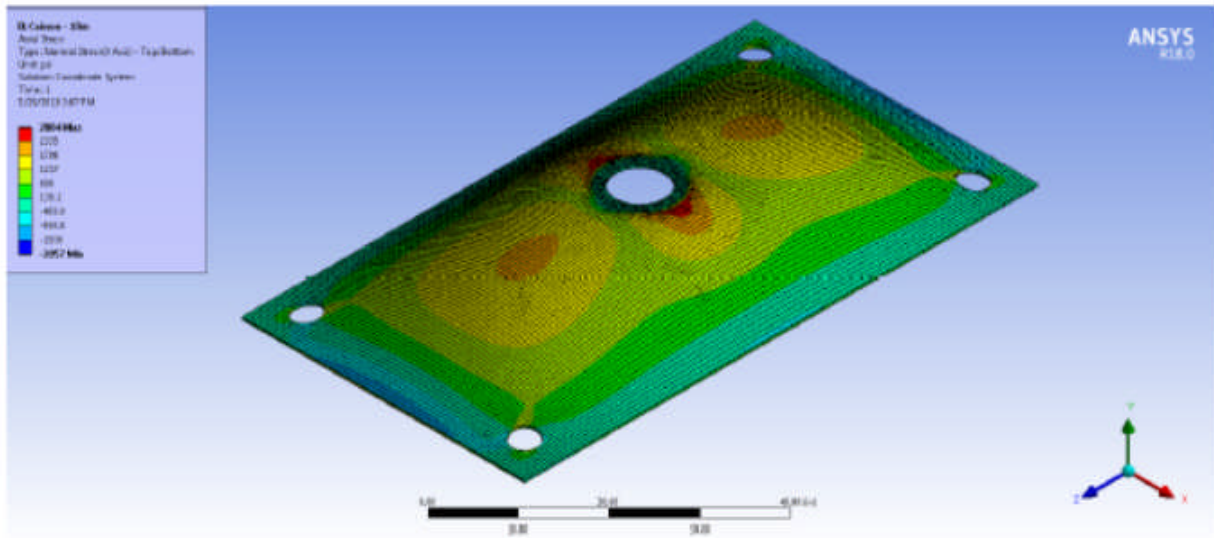


Figure 4: Axial Stress – 10m

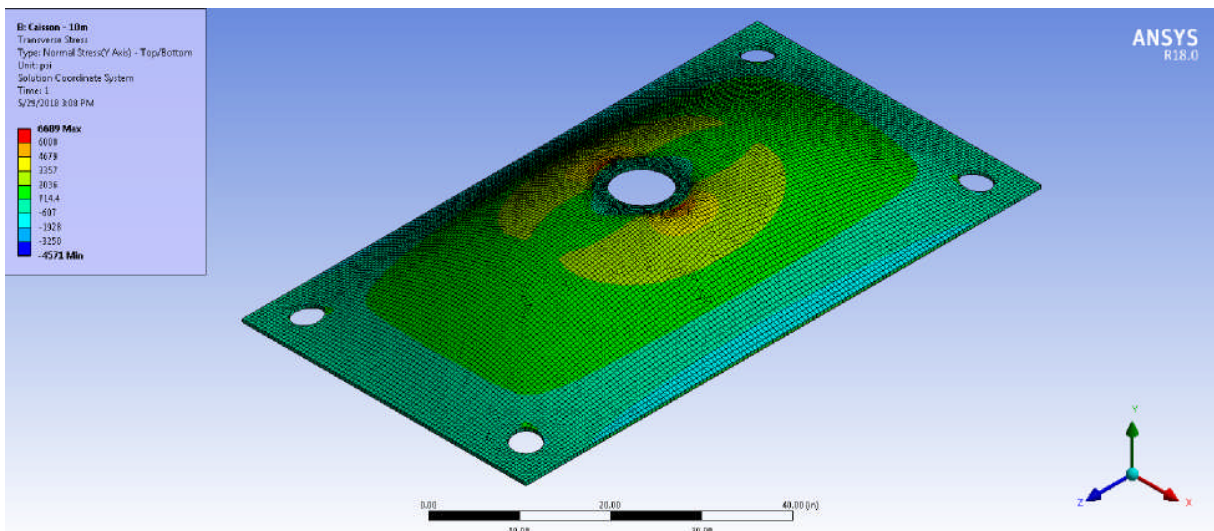


Figure 5: Transverse Stress – 10m Caisson

Highest stresses occur at the rigid flange connection at the center of the panel. While the Transverse Stress does exceed the 6000psi allowable, this stress concentration is very localized and may be a non-real stress singularity caused by the boundary condition applied at the flange. Further, more-detailed analysis may prove this is not an issue.

The plots below illustrate the Axial and Hoop Stresses (X and Y-axis material orientations) for the FW Frame beam of the 10m APEX. The FW beam is modeled as 0.55” thick. Deflection is again magnified significantly to verify load/deflection directions.

**M3 WAVE
10m & 50m APEX
FEA REPORT**

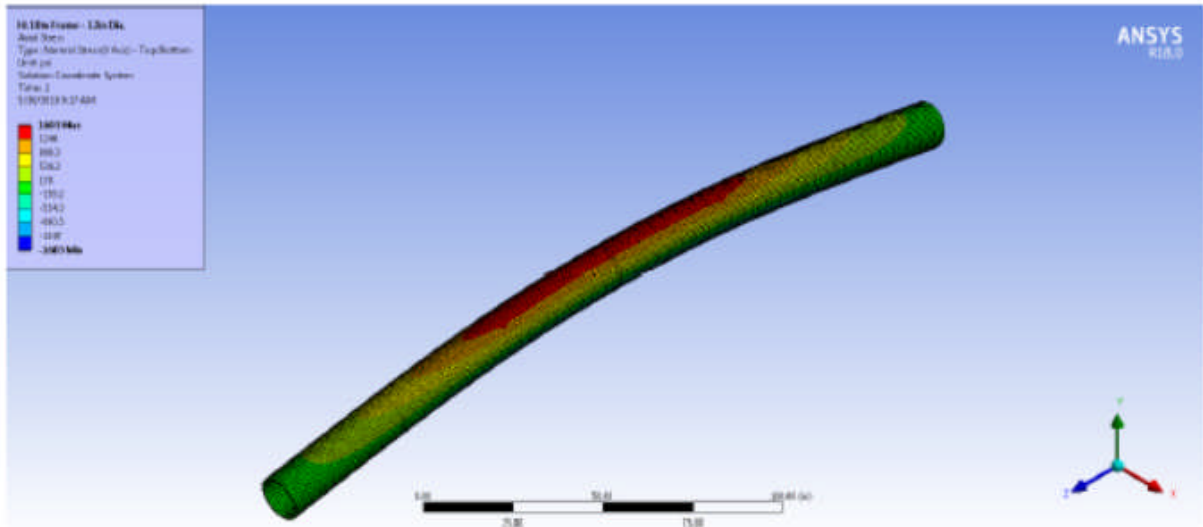


Figure 6: Axial Stress – 10m

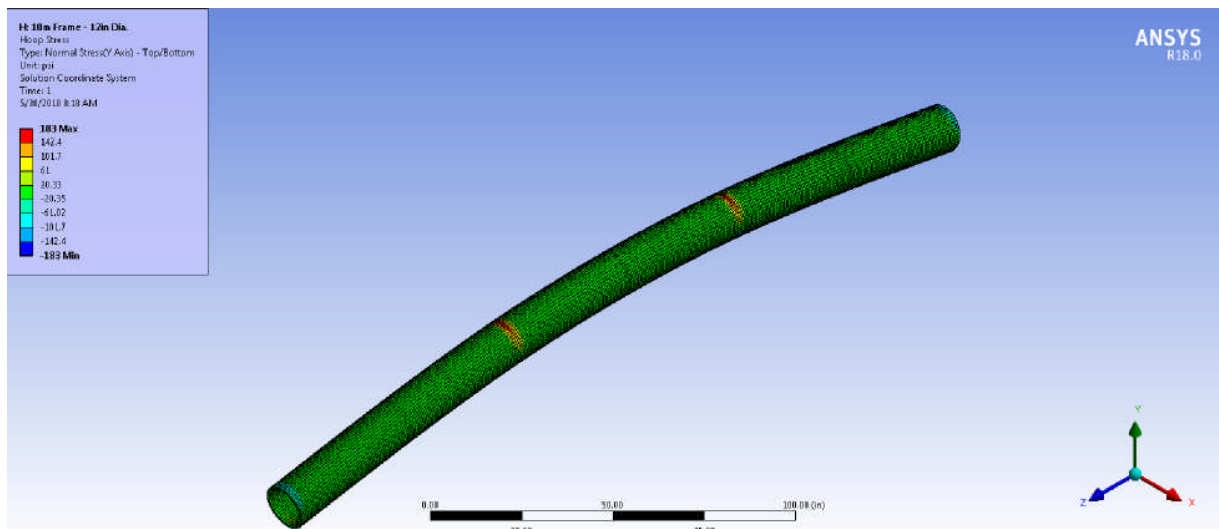


Figure 7: Hoop Stress – 10m Frame

Axial and Hoop Stresses in the FW beam are both below their respective allowable limits.

3.2 50m APEX

The following plots show the Axial and Transverse Stress in the 50m APEX Caisson panel. Material orientation and deformation magnification are as mentioned previously. The panel below is modeled as 2” thick.

M3 WAVE
10m & 50m APEX
FEA REPORT

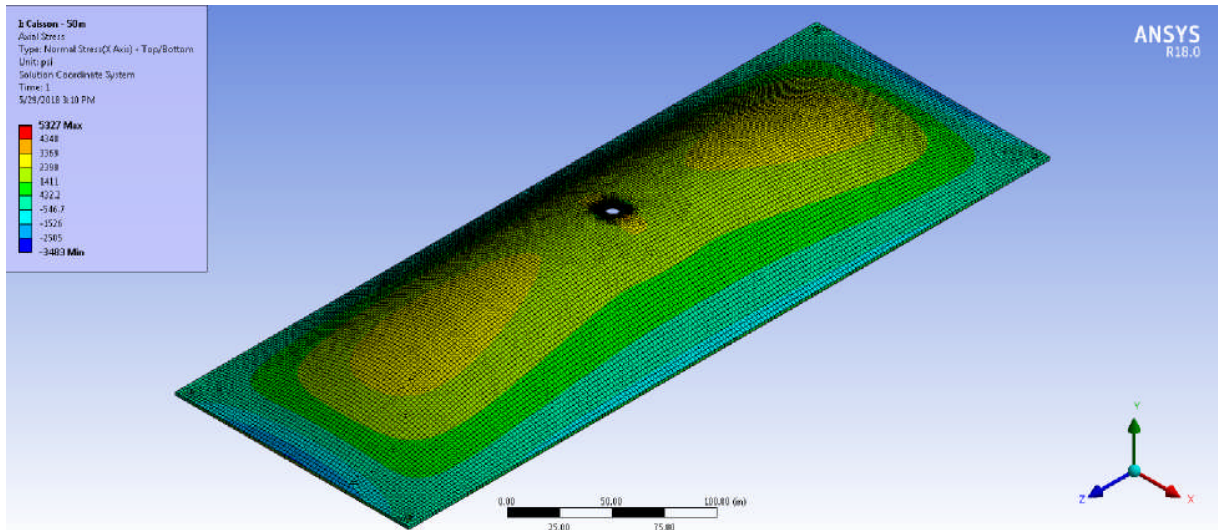


Figure 8: Axial Stress – 50m Caisson

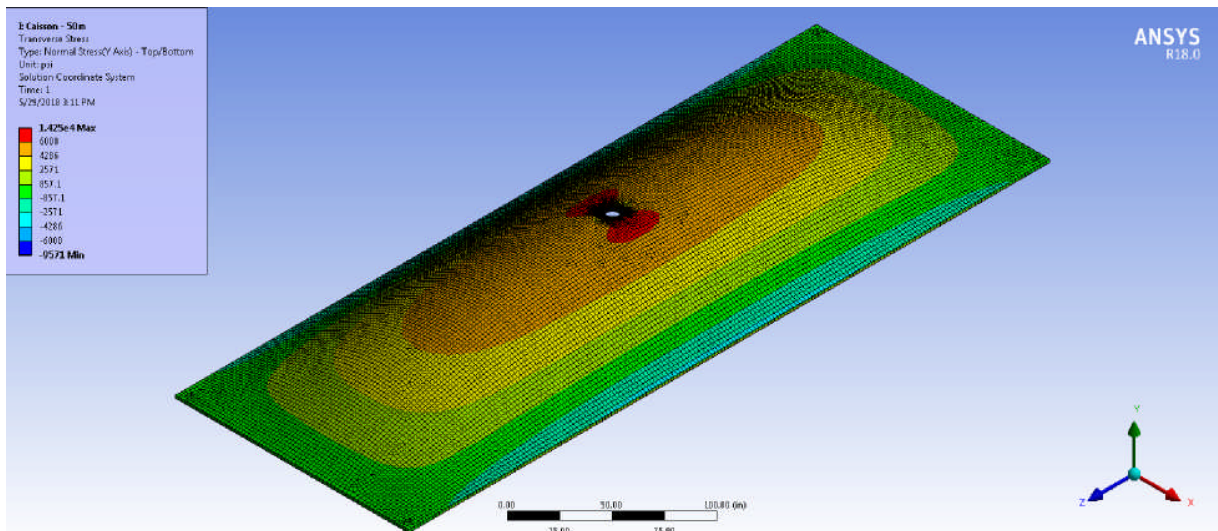


Figure 9: Transverse Stress – 50m Caisson

As before, there is an overstressed region at the flange location in the transverse direction. However, the size of the overstressed is likely more of a concern. This can likely be addressed by adding stiffeners to the panel, which would also likely serve to reduce the overall panel thickness.

The plots below show the Axial and Hoop stresses in the 50m Amex frame beam. These beams are modeled as 2.09” thick.

M3 WAVE
10m & 50m APEX
FEA REPORT

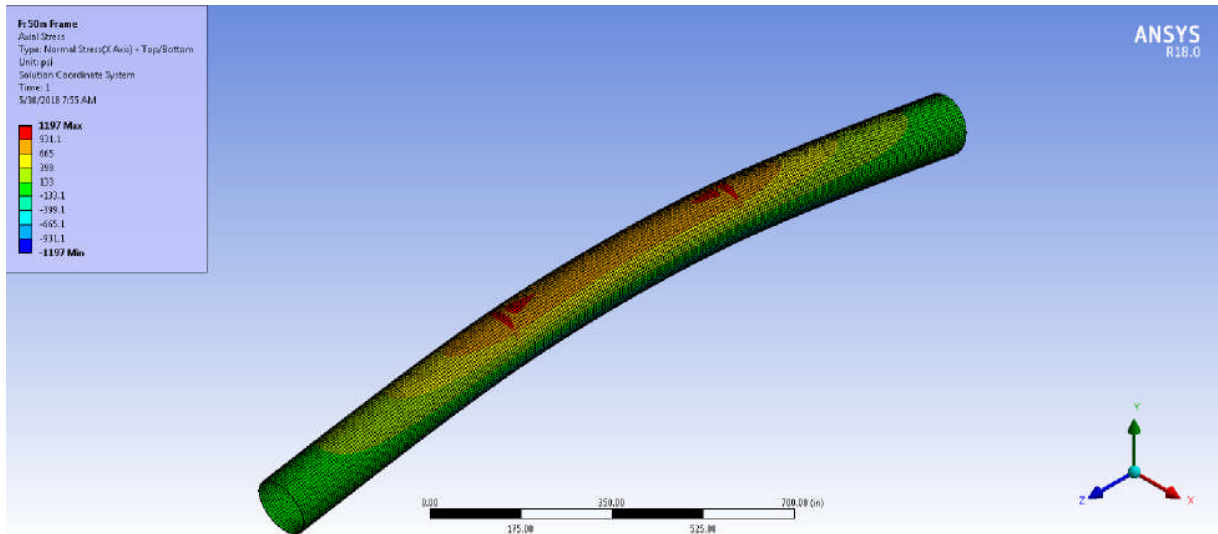


Figure 10: Axial Stress – 50m Frame

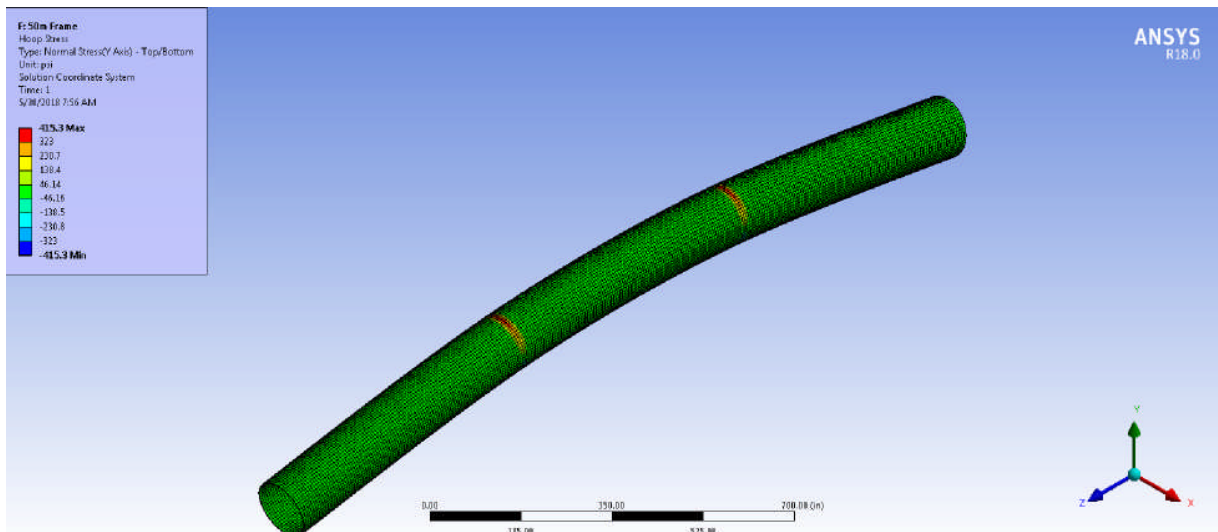


Figure 11: Hoop Stress – 50m Frame

Again, stresses in the FW beams are well below the allowable limit.

4 CONCLUSION

Based on the results (above) the conceptual thicknesses have been indicated in the 10m and 50m APEX drawing package (Rev. A, dated 4/11/18). Additional information, as it applies to these concept models, is shown below (note that this information is general approximations based on the Rev. A drawings).

M3 WAVE
10m & 50m APEX
FEA REPORT

	10m	50m
Component Weights (kips):		
Caisson	0.85	28
Frame	0.8	175
Pile Anchor	0.5	7
Total	4.5	259
Submerged Displacement (ft ³)	365	35000
Internal Volume (ft ³)	41	21000

The internal volume (above) only accounts for the volume of the frame and does not include the volume of the caissons or pile anchors as it is assumed the volume of these components will not be flooded when submerged. Also, this volume does not account for any internals or baffles that may be required within the frame which would reduce the total volume available.